

Physical Processes Leading to Extreme Day-to-day Temperature Change – Part 2: Future Climate Change

Kalpana Hamal and Stephan Pfahl

Institut für Meteorologie, Freie Universität Berlin, 12165 Berlin., Germany

5 Correspondence to: Kalpana Hamal (k.hamal@fu-berlin.de)

Abstract

Extreme temperature swings from one day to the next, whether warming or cooling, can significantly impact human health, ecosystems, and the economy. These effects may become more pronounced or attenuated in the future. Part 1 of this research identified the physical processes—advection, as well as adiabatic and diabatic temperature changes—that cause extreme day-to-day temperature (DTDT) fluctuations in the present climate. However, how these processes influence the projected change in extreme DTDT under warming scenarios remains unknown. This study addresses this question globally by analysing physical processes in Community Earth System Model Large Ensemble (CESM-LE) simulations under a high-emission scenario, employing both Eulerian composite and Lagrangian backwards-trajectory analyses. The projected changes in (extreme) DTDT variations display a seasonal contrast, weakening in mid- to high latitudes and intensification in the tropics during December–February (DJF), while during June–August (JJA), tropical intensification is more widespread, and only some extratropical locations experience reductions in DTDT variations. The spatial pattern of projected changes in the DTDT variations is mostly associated with changes in the standard deviation of daily temperature, whereas changes in temporal autocorrelation give rise to regional variation in magnitude. In the extratropics during DJF, the weakening of DTDT extremes is mainly driven by reduced advection contributions due to Arctic amplification. However, during JJA, reductions in extremes result from changes in advection, diabatic, and adiabatic processes, with differences between events and regions in their relative contributions. Furthermore, changes in diabatic processes play a significant role in the projected intensification of extremes in JJA over land areas in the tropics and subtropics, while the tropical intensification during DJF results from local changes in diabatic and adiabatic processes. Our findings demonstrate that a regional and seasonal perspective that, in addition to the well-established role of advection, also accounts for diabatic and adiabatic heating processes is essential for understanding projected extreme DTDT changes and for developing suitable adaptation strategies.

1. Introduction

In its Sixth Assessment Report, the Intergovernmental Panel on Climate Change emphasises that temperature extremes have adverse effects on human health, agriculture, and the economy, and anticipates these challenges worsening as associated weather extremes intensify (Intergovernmental Panel on Climate, 2023). Rapid day-to-day temperature (DTDT) changes, as one specific type of temperature extremes (Hamal & Pfahl, 2025), significantly impact health, primarily contributing to increased mortality rates, especially among children and older individuals (Chan et al., 2012; Hovdahl, 2022; Martínez-Solanas

Deleted: -

Deleted: -

Deleted: -

Deleted: II

Deleted: :

Deleted: I

Deleted: -

Deleted: -

Deleted: change

Deleted: -

Deleted: -

Deleted: -

Deleted: -

Deleted: clear

Deleted:

Deleted: with a dipole pattern:

Deleted: -

Deleted: during December–February (DJF),

Deleted: magnitude of

Deleted: are

Deleted: linked to

Deleted: ile

Deleted: the

Deleted: also play a role in some regions

Deleted: -

Deleted: changes in

Deleted: ,

Formatted: Numbered + Level: 1 + Numbering Style: 1, 2, 3, ... + Start at: 1 + Alignment: Left + Aligned at: 0" + Indent at: 0.25"

Deleted: -

Deleted: -

60 et al., 2021; Wu et al., 2022). They also lead to economic losses, which are notably higher at low latitudes than at high latitudes, and negatively affect agriculture (Kotz et al., 2021; Linsenmeier, 2023; Zou et al., 2024). Furthermore, these impacts are projected to increase in a warming future, particularly affecting economic activity in warm, poor regions (Linsenmeier, 2023) and being associated with reductions in cropland and yields (Wang et al., 2022). The population's exposure to the risk of these DTDT changes has continued to increase (Chen et al., 2025). Therefore, studying DTDT changes and their extremes in a
65 warming climate is **important**.

Deleted: imperative

Research on future projected changes in DTDT variations and their extremes remains limited. Zhou et al. (2020) projected a decrease in the magnitude of extreme DTDT variations across mid to high latitudes on the annual time scale, associated with declining strong wind patterns. Similar results have been observed for the Northern Hemisphere winter and summer (Kim et al., 2013; Wang et al., 2025). Xu et al. (2020) found a reduction in DTDT variations during winter and an increase along the Arctic Coast during summer, driven by notable shifts in the meridional temperature gradient. Similarly, an increase in summer variability across extratropics and tropical landmasses has been attributed to anthropogenic influences (Wan et al., 2021). All these studies have examined the typical or average magnitude and trends of DTDT changes, except for Zhou et al. (2020) and Liu et al. (2025), who also examined extreme DTDT changes using a fixed temperature threshold (Zhou et al., 2020) and a
75 percentile threshold method (Liu et al., 2025), respectively, on an annual timescale. Here, to investigate **projected** extreme DTDT changes at a seasonal timescale, a percentile-based threshold method is applied, similar to previous studies of temperature extremes in a warming climate (Schielicke & Pfahl, 2022; Vogel et al., 2020). Furthermore, we aim to investigate the detailed thermodynamic and dynamic processes underlying the projected changes in extreme DTDT variations using Eulerian composites and Lagrangian backward trajectories.

Deleted: projected future

Deleted: -

80 Backward trajectory analyses have been widely used to identify the physical processes underlying the formation of temperature extremes, encompassing advection (the transport of air from climatologically warmer regions to colder regions or vice versa), Lagrangian temperature changes associated with adiabatic compression or expansion, and diabatic heating or cooling. Such process-based analyses have been conducted both in the past (Bieli et al., 2015; Mayer, 2025; Nygård et al., 2023; Papritz & Spengler, 2017; Quinting & Reeder, 2017; Röthlisberger & Papritz, 2023a, 2023b; Zschenderlein et al., 2019) and within the context of future climate change (Brunner et al., 2018; Chan et al., 2022; Jeong et al., 2025; Schaller et al., 2018; Schielicke & Pfahl, 2022), providing a better understanding of temperature extremes. These studies also highlighted that temperature extremes are intricately linked to synoptic-scale circulation patterns, such as ridges and troughs, which control the advection of air masses and the adiabatic warming or cooling due to subsidence or ascent, respectively (Jeong et al., 2025; Kautz et al.,
90 2022; Neal et al., 2022). Additionally, turbulent mixing and diabatic processes, such as radiative cooling and sensible heat fluxes near the Earth's surface, significantly contribute to the formation of extreme temperatures (Hartig et al., 2023; Röthlisberger & Papritz, 2023a, 2023b). Future changes in extreme temperatures (daily temperature extremes and heatwaves) are primarily driven by thermodynamic processes, with less influence from dynamic processes (Brunner et al., 2018; Chan et

Deleted: -

Formatted: Font color: Red

Deleted: -

Deleted: (Hartig et al., 2023; Mayer, 2025; Röthlisberger & Papritz, 2023a, 2023b)

al., 2022; Schaller et al., 2018; Schielicke & Pfahl, 2022; Vogel et al., 2020). Here, we investigate whether this also holds for extreme DTDT changes in a warming climate.

Building on the methodology and process understanding from Part 1 of this study (Hamal & Pfahl, 2025), we investigate historical and future extreme DTDT changes in global climate simulations (i.e. Community Earth System Model Large Ensemble (CESM-LE)) using Lagrangian backward trajectory analyses of surface air masses initialised at selected locations on the two days involved in extreme DTDT changes. Furthermore, the contributions of various processes—advection, adiabatic, and diabatic warming/cooling—to projected extreme DTDT changes are analysed using a Lagrangian temperature decomposition. This study aims to address the following research questions:

- (1) What is the role of changes in atmospheric circulation patterns for projected changes in extreme DTDT variations?
- (2) Which physical processes contribute to extreme DTDT changes in a warming climate?

2. Data and methodology

2.1 CESM-LE

In this study, we use 30 ensemble members from the fully coupled 1st version of the CESM-LE project (Kay et al., 2015) to assess the influence of natural variability. The ensemble members differ by small random perturbations applied to their initial air temperature fields, with magnitudes of approximately 10^{-14} K. The simulations are externally forced using historical conditions up to 2005 and representative concentration pathway (RCP) 8.5 conditions for 2006–2100. The atmospheric variables in the CESM-LE dataset are available on a horizontal grid with approximately 1 degree spacing in latitude and 1.25 degrees in longitude, with 30 hybrid vertical levels and 6-hourly intervals. Our analysis focuses on two 10-year time slices: 1991–2000 (historical climate) and 2091–2100 (future climate). The CESM simulations were rerun for these time slices using restart files from the original CESM-LE simulations to generate additional output required for the trajectory calculations (Dolores-Tesillos et al., 2022; Schielicke & Pfahl, 2022). Afterwards, all fields were remapped to a uniform horizontal resolution of $1^\circ \times 1^\circ$. The analysis incorporates near-surface temperatures at a reference height of 2 meters above ground level, total cloud cover, precipitation, and several three-dimensional atmospheric fields, including temperature, pressure, geopotential height, and horizontal and vertical wind components. The temporal resolution of near-surface temperature and composite analyses is daily (averaged over 6-hour intervals), whereas the input data for trajectory calculations are maintained at 6-hour resolution. Previous applications of the CESM-LE for simulating temperature extremes and associated processes across various regions demonstrate its reliability and confirm its suitability for the present study (Schielicke & Pfahl, 2022; Wang et al., 2019).

Deleted: es

Deleted: Part I

Deleted: future

Deleted: projected future

Formatted: Space After: 12 pt

Deleted: -

Deleted: Community Earth System Model Large Ensemble (

Deleted: -

Deleted:)

Formatted: Superscript

Deleted: cover

Deleted: -

Deleted: -

Deleted: -

Deleted: -

Deleted: -

Deleted: -

Deleted: -

Deleted: s calculate

Deleted: from

Deleted: -

Deleted: -

Deleted: -

2.2 ERA5

We use 2m air temperature (calculated from hourly data) data from 1991 to 2000, at a spatial resolution of $1^\circ \times 1^\circ$ from the fifth-generation European Centre for Medium-Range Weather Forecasts (ECMWF) global reanalysis product (ERA5, (Hersbach et al., 2020)), to calculate present-day DTD T variability and compare it with the model simulations. More details are provided in Section 2 of Part I (Hamal & Pfahl, 2025).

2.3 Calculation of DTD T changes and their extremes

The DTD T change, δT , is defined as the difference in daily mean near-surface air temperature between the day of the event (t) and the previous day ($t-1$). Here, T_{t-1} and T_t represent the near-surface air temperatures on these two days, respectively. The standard deviation of the DTD T change σ_{DTDT} can be expressed as a function of the usual standard deviation σ_T and the lag-1 autocorrelation $r_{1,T}$ of the daily mean temperature, as indicated in Eq. (1), which was derived in Section 2 of Part I (Hamal & Pfahl, 2025). We calculate all these quantities for the historical and future scenarios for each ensemble member, then determine the differences between each member's scenarios and the ensemble mean.

$$\sigma_{DTDT} = \sigma_T \sqrt{2(1-r_{1,T})} \quad (1)$$

Extreme DTD T changes are examined using the percentile method for both historical and future climates. Cooling and warming events are determined at each grid point and for each ensemble member, using the 5th and 95th percentiles of DTD T change as thresholds. The analysis focuses on two seasons: December–February (DJF) and June–August (JJA). At each location, 44 events are selected for DJF and 45 for JJA for each member and each ten-year time slice (historical and future climate).

2.4 Trajectory calculation

We employ a Lagrangian analysis method to compute backwards trajectories, similar to the approach used for ERA5 in (Hamal & Pfahl, 2025), but here applied to each CESM-LE's historical and future extreme DTD T changes during both days $t-1$ and t , respectively. 3-day backward trajectories are initialised at 18 UTC from pressure levels of 10, 30, 50, and 100 hPa above the surface at each selected grid box (see section 2.5). Output data, including latitude, longitude, pressure, temperature, and potential temperature, are recorded at 6-hour intervals. We then compare the trajectories for extreme events in the historical and future scenarios to assess their projected changes.

Trajectory density was quantified using two-dimensional Kernel Density Estimation applied to the geographic coordinates of back-trajectory positions at 3d. The KDE was evaluated on a common fixed grid over the selected locations, ensuring spatial consistency and direct comparability across all cases and ensemble members. The resulting density field was normalised by

Deleted: utilise

Deleted: 1980

Deleted: 20

Deleted: -

Deleted: -

Deleted: -

Deleted: Part I

Deleted: -

Deleted: -

Deleted: -

Deleted: -

Deleted: Part I

Deleted: the scenarios for

Deleted: -

Deleted: key

Deleted: -

Deleted: -

Deleted: -

Deleted: -

Deleted: -

Formatted: English (UK), Not Highlight

200 the total density sum and expressed as a percentage (%), representing the relative frequency of air mass occurrence at each grid point.

Formatted: English (UK)

Formatted: English (US)

2.5 Lagrangian temperature decomposition

205 To better understand the underlying mechanisms of extreme DTD T changes, our analysis focuses on different locations that show significant projected changes during DJF and JJA. For DJF, we select two locations: North America (51°N, 86°W) and tropical South America (13°S, 56°W), whereas for JJA, we focus on western North America (45°N, 120°W) and central Europe (50°N, 10°E) in the main paper. Additional grid points are shown in the supplementary material. At these locations, the Lagrangian decomposition method (eq. 2) developed in Part 1 (Hamal & Pfahl, 2025) is utilised to quantify the contributions of advection, adiabatic, and diabatic processes to extreme DTD T changes in both historical and future scenarios. This method is applied to 3-day backward trajectories initiated during the two days associated with extreme DTD T change events in both present and future climates.

Deleted: projected future

Deleted: in Northern Asia (70°N, 90°E), Northern Europe (60°N, 10°E), tropical Southern Africa (13°S, 24°E) for DJF, eastern North America (41°N, 76°W), Southern Asia (35°N, 80°E), the Sahel region (15°N, 5°E), Southern South America (47°S, 70°W), Northern Asia (68°N, 80°E) and Southern South Africa (30°S, 22°W) for JJA ...

Deleted: Part I

Deleted: -

$$\delta_T^0 \approx \delta_T^{-3d} + \delta_T^{adi} + \delta_T^{dia} + res \quad (2)$$

215 Here, the DTD T change (δ_T^0) is decomposed into three contributing factors with full integral expressions calculated as in Part 1 (equations A4-6 in (Hamal & Pfahl, 2025)). The mean here refers to the trajectory-average value of each process.

Deleted: (

Formatted: Font color: Auto, English (US)

Formatted: Font color: Auto, English (US)

Formatted: Font color: Auto, English (US)

Formatted: Font color: Auto, English (US)

Formatted: Font: Font color: Auto, English (US)

Formatted: Font: Font color: Auto, English (US)

Deleted: :

Deleted: t

Formatted: Font color: Auto, English (US)

Formatted: Font: Italic

220 The mean temperature difference at the origin of the air masses three days before initialization, which indicates the contribution of changes in advection change (δ_T^{-3d}), a contribution of mean adiabatic compression or expansion change resulting from vertical descent or ascent (δ_T^{adi}), and a contribution of mean diabatic heating or cooling change from processes such as latent heating in clouds, radiation, and surface fluxes (δ_T^{dia}). The final term is the residuum change (res), resulting from numerical inaccuracies in the calculations. The residual change is usually small and therefore not further addressed in the subsequent text and figures. Equation (2) is applied separately for the historical and future climate, and projected changes in the contributions are calculated as differences between the time slices.

225 Furthermore, to determine the contribution of Arctic Amplification (AA) to changes in extreme DTD T events, we compare the seasonal mean temperature change at the air parcels' origin points (-72h) between days t and $t-1$. To determine the origin, we use historical trajectory pathways, neglecting projected changes in circulation and thereby isolating the effect of seasonal-mean background warming in the source regions. As the mean latitude of the source regions typically changes between $t-1$ and t , this differential warming is due to AA.

230

2.6. Statistical test

To quantify observational uncertainty in the historical climate, we generate a probability distribution by bootstrapping the ERA5 dataset: randomly selecting 10 years from ERA5 to obtain one sample of a 10-year average variable (e.g., DTD), and repeating this procedure $n=1000$ times. A 10-year average is used because the 10-year historical time slice is available from CESM-LE (see again section 2.1). This distribution is then compared with the variability represented by the CESM-LE multi-member ensemble, which is sampled in a similar manner by pooling all ensemble members from the historical simulations. To assess projected climate change, we employ the same bootstrap approach, comparing all pooled ensemble members from the historical and future climate simulations. The statistical significance of these bootstrap results is then evaluated using a false discovery rate (FDR) correction (Wilks, 2016) at the 1% significance level. For the composite maps, statistical significance is determined using a two-sample t -test, and we only display differences that exceed the 95% confidence threshold.

3. Result

3.1 Projected DTD changes in DJF and JJA

During the historical climate period, temperature variability in the CESM-LE simulations, quantified through both σ_{DTDT} and σ_{T_s} , is typically larger in the mid- to high latitudes of both the Northern and Southern Hemispheres than in the tropics. This pattern is consistently observed during DJF and JJA (Figures 1a-b and 2a-b). The model captures large-scale spatial patterns (cf. Part I); however, the magnitude lies outside of the non-parametric bootstraps resampling based on ERA5 in many regions (stippling in Figures 1a-b and 2a-b). Approximately 40–70% of global land regions exhibit systematic biases in daily temperature and related metrics simulated by CESM-LE relative to ERA5 (Fig. S1). Notable biases include large parts of the Northern Hemisphere mid- and high latitudes and Southeast Asia during DJF (Figures 1a-b), where the model overestimates variability, and several subtropical regions during JJA (Figures 2a-b and Fig. S1). In contrast, the model underestimated variability in the tropics and at most JJA locations. The simulated autocorrelation generally agrees well with ERA5 (Figures 1c, 2c), though there are regional exceptions, notably in the deep tropics, Central America, and the Arabian Peninsula, where it shows positive biases (Fig. S1c and f). Furthermore, in CESM-LE, the spatial pattern σ_{DTDT} is generally contributed by σ_T (as outlined in Eq. 1), with the influence of $r_{1,T}$ being restricted to the regional scale, as discussed for ERA5 in Part I.

Formatted: Heading 2

Deleted: future

Deleted: -

Deleted: σ_{T_s}

Deleted: -...to...high latitudes of both the Northern and Southern Hemispheres compared...han to...n the tropics. This pattern is consistently observed during DJF and JJA (Figures 1a-...b and 2a-...b). ...he model

Formatted

Deleted: results ...agnitude lies outside of the non-parametric within ...ootstraps resampling $\pm 10\%$ of estimates ...ased on ERA5 (cf. Part I) ...n many regions (stippling in Figures 1a-...b and

Formatted

Deleted: , which enhances confidence in its projections. Notable Notable biases exceptions ...nclude large parts of the Northern Hemisphere mid-... and high latitudes and Southeast Asia during DJF (Figures 1a-...b), where the model overestimates variability, and several subtropical regions during JJA (Figures 2a-...b and Fig. S1). In contrast, the model underestimated variability in the tropics and at most JJA locations. The simulated autocorrelation generally ...grees well with ERA5 (Figures 1c, 2c), though there are regional exceptions, notably in the deep tropics, Central America, and the Arabian Peninsula, where it shows positive biases (Fig. S1c and f). Furthermore, also ...n CESM-...LE, the spatial patter

Deleted: determined by

Formatted

Deleted: s

Deleted: $r_{1,T}$

Deleted: Part I

Formatted: Font: Italic

385 Australia. Also, in the future, the pronounced σ_{DTDT} changes are also primarily associated with changes in σ_T . Although the
changes $\tau_{1,T}$ are relatively modest (10–20%, Fig. S2c), they introduce important regional variations in the magnitude of the
390 response, particularly in the Northern Hemisphere midlatitudes and the tropics (Figure 1f). For example, in regions such as
North America and northwestern Asia, small σ_T magnitude combined with a slight increase in autocorrelation is linked to a
more pronounced decline in σ_{DTDT} (see Eq. 1). In these areas, the DTD distribution is projected to become narrower and
more peaked, accompanied by increases in skewness and kurtosis (Fig. S4a). Conversely, in the deep tropics, the projected
395 magnitude σ_{DTDT} changes are slightly larger relative to the change in σ_T due to reduced autocorrelation. In these regions, the
historically low variability and sharply peaked distribution are projected to broaden, with reductions in kurtosis and skewness
(Fig. S4b).

During JJA, most regions globally are projected to experience an increase in σ_{DTDT} (Figure 2d–e) exceeding 20% in many
400 areas (Fig. S2d–e). The increases in σ_{DTDT} in regions such as Europe, the Amazon, the Sahel, the Maritime Continent, southern
Australia, South and Southeast Asia, Central America, and parts of northern Russia are associated with concurrent increases
in σ_T . In these regions, changes in the distribution's shape are also evident, with notable shifts in kurtosis and skewness (Fig.
S4d) and slight changes in autocorrelation (Figure 2f). Only in a few regions, σ_{DTDT} variability is projected to decrease by
405 more than 10% (Figure 2d and Fig. S2d). Over parts of western and eastern North America, Northeastern Asia and
Greenland, σ_{DTDT} projections are expected to decrease despite smaller changes or even a slight increase in σ_T , which is due to
significant increasing $\tau_{1,T}$ (Figures 2d–f, Eq. 1). The inter-model variations of the JJA response are relatively small (Fig. S3d–
f).

- Deleted: The
- Deleted: changes
- Deleted:
- Deleted: driven by
- Deleted: , as $\tau_{1,T}$ does not exhibit significant changes (Figure 1f).
- Formatted: Font: 10 pt
- Formatted: Font: 10 pt
- Formatted: Font: 10 pt
- Formatted: Font: 10 pt
- Formatted: Font: 10 pt
- Formatted: Font: 10 pt
- Formatted: Font: (Default) Times New Roman, Font color: Auto
- Formatted: Font: (Default) Times New Roman, Font color: Auto
- Formatted: Default Paragraph Font, Font: (Default) Times New Roman, Font color: Auto
- Formatted: Font: (Default) Times New Roman, Font color: Auto
- Formatted: Default Paragraph Font, Font: (Default) Times New Roman, Font color: Auto
- Formatted: Default Paragraph Font, Font: (Default) Times New Roman, Font color: Auto
- Formatted: Font: (Default) Times New Roman, Font color: Auto
- Formatted: Font: (Default) Times New Roman, Font color: Auto
- Formatted: Font: (Default) Times New Roman, Font color: Auto
- Formatted: Font: (Default) Times New Roman, Font color: Auto
- Formatted: Font: (Default) Times New Roman, Font color: Auto
- Formatted: Font: (Default) Times New Roman, Font color: Auto
- Formatted: Default Paragraph Font, Font: (Default) Times New Roman, Font color: Auto
- Formatted: Font: (Default) Times New Roman, Font color: Auto
- Formatted: ... [11]
- Formatted: ... [12]
- Formatted: ... [13]
- Formatted: ... [14]
- Formatted: ... [15]

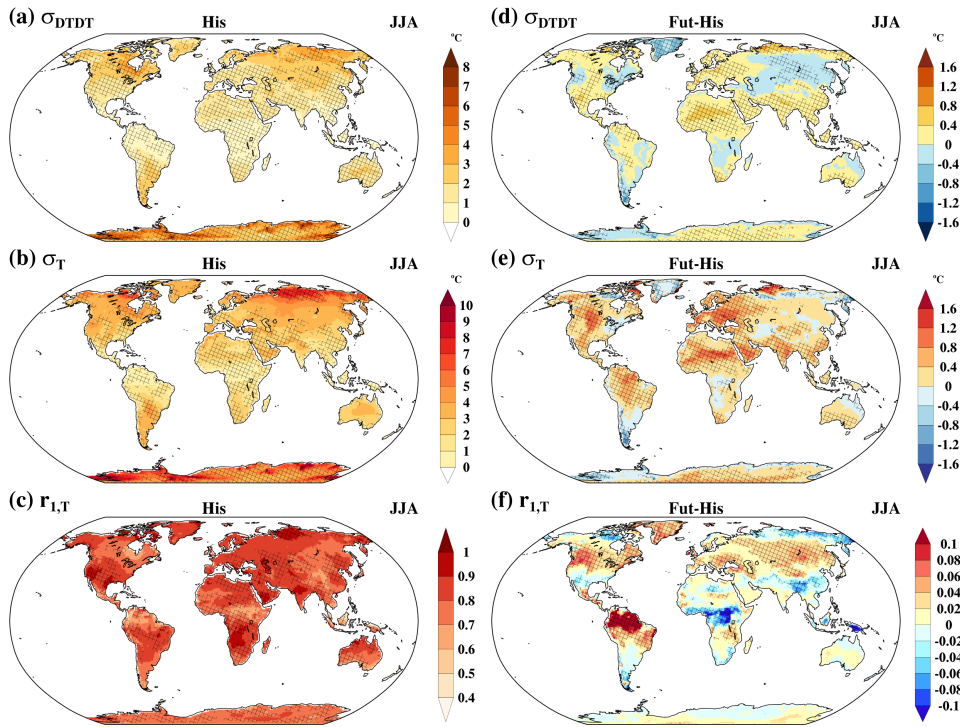
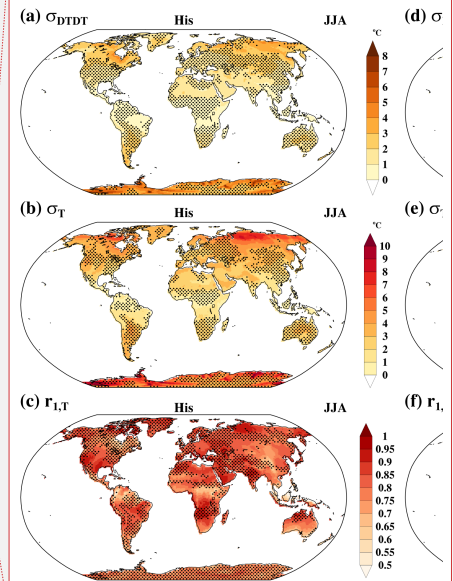


Figure 2. The ensemble means of (a, d) standard deviation of DTD variations (σ_{DTDT} , °C), (b, e) standard deviation of daily mean temperature (σ_T , °C), and (c, f) lag-1 autocorrelation of daily mean temperature ($r_{1,T}$) in June–August (JJA) in the historical climate (a–c) and projected change (d–f). In the panels (a–c), cross-hatching marks grid points where the CESM-LE ensemble mean differs significantly from the ERA5-derived metric, with statistical significance determined through bootstrap resampling. In panels (d–f), cross-hatching denotes grid points where the future minus historical difference is significantly different from zero, assessed via a two-sample bootstrap test.

3.2 Projected extreme DTD changes

The 5th and 95th percentiles serve as thresholds at each grid point to identify historical and projected extremes of DTD cooling and warming, as depicted in Figure 3. In DJF, the model overestimates the historical magnitudes of warming and cooling events in the subtropics and mid- to high latitudes, but underestimates them in the tropics relative to ERA5. By contrast, JJA is characterised by a widespread underestimation of these events, except for overestimations observed in arid regions and high latitudes (Stippling in Figures 3a–d). The future patterns of extreme DTD changes closely correspond with

Deleted: with a few regional exceptions such as an area in tropical western Africa, where σ_{DTDT} increases due to a reduction of $r_{1,T}$ in spite of minor changes in σ_T (see again Eq. 1).



Formatted: Justified

Formatted: Caption

Deleted: -

Deleted: -

Deleted: -

Deleted: future

Deleted: -f

Deleted: Stippling indicates locations where at least 80% of CESM-LE members lie within $\pm 10\%$ of the ERA5-derived respective quantities, indicating model consistency with observations. Meanwhile, for the projected future change, stippling indicates areas where $\geq 80\%$ of ensemble members agree on the sign of change.

During JJA, most regions globally are projected to experience either minor changes or an increase in both σ_{DTDT} and σ_T (16)

Deleted: †

Deleted: future

Formatted: Justified

the projected climatological σ_{DTDT} and σ_T patterns (Figures 1, 2, and 3). During DJF, the areas where historical extreme DTD T changes have the highest magnitude, primarily in mid- to high latitudes, are expected to experience a decrease in intensity in the future (Figures 3e-f). In contrast, in tropical regions, these extremes are projected to intensify. In JJA, projected changes exhibit regional variations, with intensities mainly increasing in parts of the tropics and subtropics. Exceptions with weakening extreme DTD T changes are observed in some extratropical regions, including western and eastern North America, Northeastern Asia, Greenland, and Southern South America (Figures 3g-h).

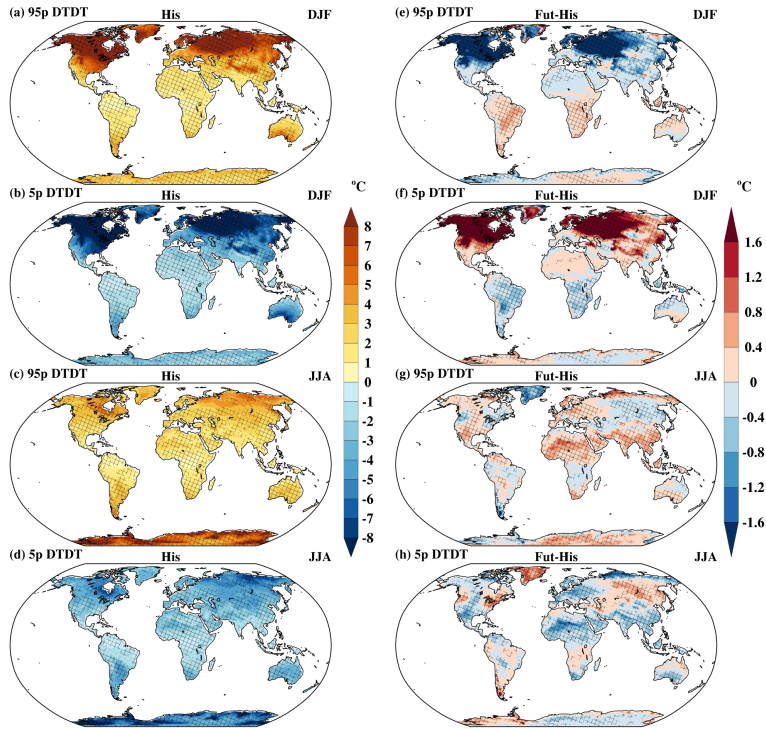
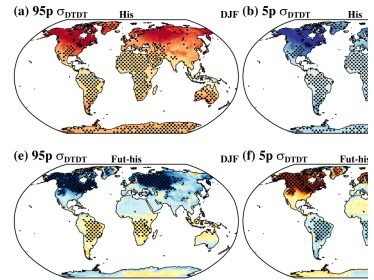


Figure 3. The ensemble means of the (a, c, e and g) 95th percentile (95p) and (b, f, d and h) 5th percentile (5p) of DTD T variations during (a, b, c, e, f) December, February (DJF) and (c, d, g, h) July, August (JJA) based on the historical climate (a-d) and projected change (e-h). In panels (a-c), cross-hatching marks grid points where the CESM-LE ensemble mean differs significantly from the ERA5-derived metric, with statistical significance determined through bootstrap resampling. In panels (d-f), cross-hatching denotes grid points where the future minus historical difference is significantly different from zero, assessed via bootstrapping.

Deleted: ... to high latitudes, are expected to experience a decrease in intensity in the future (Figures 3e-...f). In contrast, in tropical regions, these extremes are projected to intensify. In JJA, projected future...rojected changes exhibit regional variations, with intensities mainly increasing in parts of the tropics and subtropics. Exceptions with weakening extreme DTD T changes are observed in some extratropical regions, including western and eastern North America, Northeastern Greenland...sia, Greenland, and Southern South America Chile ...Figures 3g-...h). (... [18])



Deleted:
Formatted: Space Before: 0 pt, After: 0 pt, Line spacing: 1.5 lines

Formatted (... [19])

Deleted: -... , e- (... [20])

Deleted: -

Deleted: -... , g- (... [21])

Deleted: -

Deleted: -

Deleted: future

Deleted: -

Deleted:

Formatted: Font: 9 pt

Formatted: Font: 9 pt, Not Bold

Formatted: Font: 9 pt

Formatted: Font: 9 pt, Not Bold

Formatted: Font: 9 pt

Formatted: Font: 9 pt, Not Bold

Formatted: Font: 9 pt, Not Bold

Formatted: Normal

470

475

480

3.2.1 Projected weakening of extreme DTD changes

During DJF, the northern mid- to high-latitude regions (North America, Northern Asia, and Northern Europe) are projected to experience a decrease in extreme DTD changes compared to the historical climate, driven by consistent changes in atmospheric circulation and physical processes, as illustrated in Figures 4–6 and Figs. S5–11. This section focuses exclusively on the results for North America. Composites of anomalies from the seasonal climatology are shown for both days involved in an extreme DTD change for geopotential height (GP) at 500 hPa, wind at 850 hPa, and sea level pressure (SLP) in Figure 4, together with changes in the day-to-day circulation differences in Fig. S5.

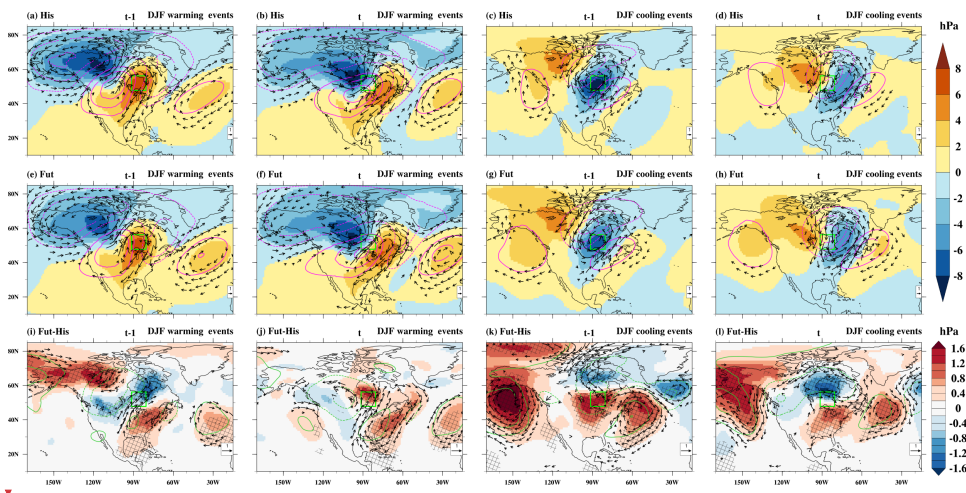


Figure 4. Composite of sea level pressure anomalies (hPa, color shading), wind anomalies at 850 hPa ($m s^{-1}$, vectors), and geopotential height anomalies at 500 hPa (gpm, magenta and dark green contours) relative to the seasonal mean on the (a, e, i, c, g, k) previous day ($t-1$) and (b, f, j, d, h, l) the event day (t) of the warming (a–b, e–f and i–j) and cooling (c–d, g–h and k–l) events during December–February (DJF) in (a–d) historical climate (His), (e–h) future climate (Fut), and (i–l) projected changes (Fut–His) at a selected grid box in North America (green box). Note that, in (a–h), wind vector anomalies $\geq 2 m s^{-1}$ and in (i–l), wind vector difference anomalies $\geq 0.5 m s^{-1}$ are plotted. The dotted and bold contours indicate negative and positive geopotential height anomalies, respectively. Additionally, the cross-hatching area indicates where the ensemble mean of sea level pressure differences exceeds the 95% confidence threshold based on a t -test.

In the simulated historical period, DTD warming events are associated with pronounced shifts in GP, SLP, wind anomalies, and air mass origin between days $t-1$ and t (Figures 4a–b and 5a–b). On day $t-1$, the grid box lies within a high-pressure area downstream of an eastward-propagating ridge at 500 hPa, in a transition zone between southwesterly wind anomalies to the west and northeasterlies to the east (Figure 4a), associated with the advection of relatively cool air masses (Figures 5a, m). By day t , the ridge moves over the grid box, featuring southwesterly wind anomalies in between an upstream surface low and the

Deleted: Stippling indicates locations where at least 80% of CESM-LE members lie within $\pm 10\%$ of the ERA5-derived respective quantities, indicating model consistency with observations. Meanwhile, for the projected future change, stippling indicates areas where $\geq 80\%$ of ensemble members agree on the sign of change.

Deleted: future

Formatted: Default Paragraph Font

Deleted: -

Deleted: -

Deleted: -

Deleted: e

Deleted: rn

Deleted: -

Deleted: 4-

Deleted: 6

Deleted: -

Deleted: -

Deleted: 4

Deleted: 1

[22]

Deleted: -

Deleted: -

Deleted: -

Deleted: -

Deleted: -

Deleted: -

Deleted: -

Deleted: -

Deleted: -

Deleted: -

Deleted: -

Deleted: future

Deleted: -

Deleted: -

Deleted: -

Deleted: -

Deleted: hatched

Deleted: Student's

Deleted: -

Deleted: 1

Deleted: In the simulated historical period, DTD warming events are associated with pronounced shifts in GP, SLP, wind and ... [23]

high that shifted downstream (Figure 4b) and the advection of much warmer continental air masses (Figures 5b, m). This shift to southwesterly advection (see also Fig. S5a) contributes an average warming of +6.2°C to the DTD T change (Figures 5m and 6a). Those events also show a large change in the local temperature gradient, indicating a relation with advection (Fig. S7a). In terms of vertical transport, weaker subsidence at t compared to $t-1$ reduces the adiabatic warming by -2.6°C (Figures 5i, 6a), partially offsetting the temperature increase. Conversely, enhanced diabatic heating during the final 24 hours of the event day contributes +4.8°C to the DTD T change (Figure 5q), further amplifying the warming. The strength of these process contributions varies across events, as illustrated by the box-and-whisker plots (Figure 6a). In summary, the simulated DTD T warming events during the historical period are primarily driven by a shift toward southwesterly warm-air advection, with diabatic heating reinforcing the effect and adiabatic changes slightly dampening it (Figure 6a). These model results generally align with the patterns and process contributions identified from ERA5 reanalysis data (see Figures 4a-c and 5k in Part 1). A quantitative comparison indicates that CESM-LE exhibits slightly smaller advection (due to less southerly flow), along with greater reduced adiabatic and diabatic contributions than ERA5.

In general, the future synoptic-scale pattern for DTD T events resembles the historical pattern, though SLP and GP anomalies weaken and shift southeastward, indicating more rapid circulation propagation (Figure 4e-f). This faster progression leads to an earlier shift to southwesterly flow at $t-1$, shifting air mass origins southwestward (Figures 4i, 5e). By day t , GP anomalies move further downstream, enhancing southerly meridional flow (Figures 4j, 5f). Thus, both days exhibit a stronger southerly component, though the southwesterly strengthening is more pronounced at $t-1$, resulting in a northeasterly anomaly between days (Fig. S5c). These relatively subtle changes in circulation patterns are associated with an average net reduction of -1.1°C in the advective contribution to DTD T warming compared to the historical period (Figure 6c). This advective reduction is because the projected warming at the origin of the traced air masses (at $t-3d$) is 9.4°C at $t-1$ but only 8.3°C at t (Figure 5n), which is both considerably above global mean warming (Figs. S6a-c). Nevertheless, from Arctic Amplification alone, one would expect an even larger reduction of the advective contribution (Figs. S7a and c), indicating that changes in circulation mitigate the effect of AA (Figs. S7a and c). Furthermore, projected changes in vertical motion indicate slightly increased subsidence on day $t-1$ (by 5-6 hPa in 3d, Figure 5j) compared to day t , which modestly enhances adiabatic warming, reducing the warming between $t-1$ and t by an additional -0.5°C. Diabatic heating decreases relative to the historical period on both days, with a slightly larger reduction on the event day (mainly in the last 24h before arrival; Figure 5r), contributing an additional -0.5°C to the overall decrease in warming. Overall, the weakening of all three contributions together results in a mean reduction in the DTD T warming of -2.1°C, with the reduced advective contribution accounting for approximately half of this signal. However, changes in diabatic and adiabatic warming also play a significant role (Figure 6c).

Deleted: In general, the synoptic-scale flow pattern associated with future DTD T warming events (Figure 4e-f) is similar to the historical pattern. However, there are signals that SLP and GP anomalies are predicted to weaken and shift southeastward relative to the historical period (Figure 4i-j), indicating a more rapid propagation. This faster propagation leads to an earlier shift to southwesterly flow toward the selected location, resulting in southwesterly wind anomalies and a southwestward change of air mass origins relative to the historical simulation at $t-1$ (Figures 4i, 5e). On day t , the further downstream location and slight change in the orientation of the GP anomalies (Figure 4j) are associated with an enhanced meridional flow of southerly air masses into the region (Figures 4j, 5f). Hence, on both days involved in future DTD T warming events, the flow has a stronger southerly component. Still, the strengthening of the southwesterlies is more pronounced at $t-1$; the difference between the two days thus shows a northeasterly anomaly (Fig. S4c).

Deleted: future

Deleted: -

Deleted: -

Deleted: .

Deleted: In addition to changes in the wind (with stronger southerlies in particular at $t-1$), future changes in the meridional temperature gradient may contribute to this differential warming, with Arctic amplification being expected to lead to larger warming in the still more northerly source regions at $t-1$

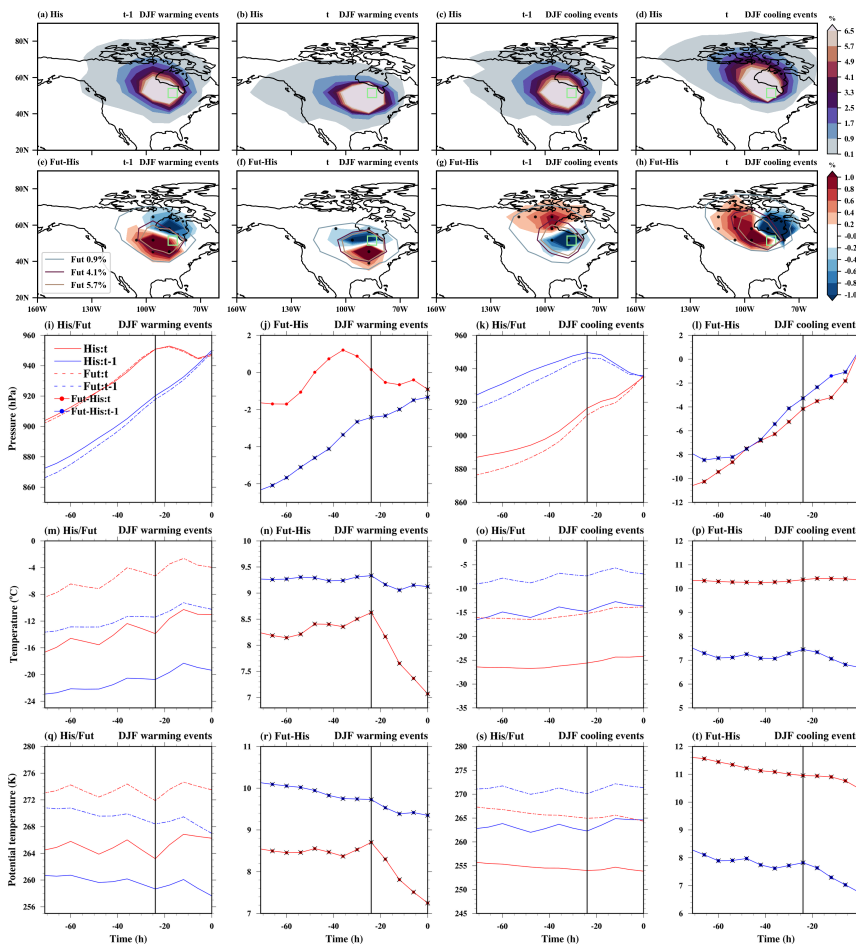
Deleted: compared to t (see Figures 4i-j and 5e-f). P

Deleted: -

Deleted: -

Deleted: ¶

Deleted: ' ... [24]



680 **Figure 5.** The spatial distribution of trajectory density initiated on the previous day ($t-1$) and the event day (t) is depicted for both December-February (DJF) warming and cooling events over North America (green box). Color shading shows the air mass density (%) during the 3d before arriving at the target grid box for (a, d) historical climate and (e, h) projected change. In (e, h), stippling areas indicate where the ensemble mean of density differences exceeds the 95% confidence threshold based on a t -test. The contours outline the 0.9%, 4.1%, and 5.7% levels of future trajectory density. The mean Lagrangian evolution of distinct physical parameters (pressure, temperature, and potential temperature) is shown along the air mass trajectories initialised on the previous and event days for historical/future extreme events (1st and 3rd columns) and projected changes in extremes (2nd and 4th columns). Additionally, bold circles with crosses show where the ensemble mean differences at each timestep exceed the 95% confidence threshold based on a t -test.

- Deleted: -
- Deleted: -
- Formatted: Font: Bold
- Formatted: Font: Not Bold
- Formatted: Font: Not Bold, Italic
- Formatted: Font: Not Bold
- Formatted: Font: Not Bold
- Formatted: Font: Not Bold
- Deleted: -
- Deleted: -
- Deleted: future
- Deleted: -
- Formatted: Font: Not Bold
- Formatted: Font: Not Bold
- Formatted: Font: Not Bold
- Formatted: Font: Not Bold
- Formatted: Font: Not Bold
- Formatted: Font: Not Bold
- Formatted: Font: Not Bold
- Deleted: s
- Deleted: areas where
- Deleted: $\geq 80\%$ of the ensemble members agree on the sign of change...
- Deleted:
- Formatted: Font: Bold
- Formatted: Font: Bold, Not Superscript/ Subscript
- Formatted: Font: Bold
- Deleted: bold circles
- Formatted: Font: Bold, Not Superscript/ Subscript
- Formatted: Font: Bold
- Formatted: Font: Bold
- Formatted: Font: Bold, Not Superscript/ Subscript
- Formatted: Font: Bold
- Deleted: Student's
- Deleted: -

705 During historical DTD T cooling events, a southeastward transition of a trough-ridge pattern and associated SLP anomalies
between days $t-1$ and t dominate the temperature drop (Figures 4c-d, 5c-d, and Fig. S5b). Specifically, the shift from a
southwesterly advection of a warm air mass downstream of a low-pressure anomaly on day $t-1$ to northerly transport of a
colder air mass between an upstream surface high and the downstream low on day t drives the cooling. This pattern results in
a large advective contribution of -9.8°C to the temperature decrease (Figures 5o and 6b). The advective cooling is partially
offset by moderate adiabatic warming ($+2.9^{\circ}\text{C}$), resulting from enhanced subsidence and descent of air masses on the event
710 day (Figures 5k and 5o). Additionally, diabatic cooling on day t contributes -2.4°C (Figure 5s), further intensifying the overall
temperature decline. Collectively, the strong cold-air advection, reinforced by diabatic cooling, is the primary driver of DTD T
cooling events across North America and other mid- to high-latitude regions (Figures 6b and Figs. S5-S11). A comparison of
North American cooling events shows that, while diabatic cooling is similar between CESM-LE and ERA5. Cold-air
advection is slightly weaker (the flow is less northerly), and the adiabatic process is marginally more pronounced (due to
715 descent from a higher level) compared to the ERA5 (see Figures 4d-f and 5l in Part I).

720 The synoptic circulation characterising future DTD T cooling events is very similar to the historical events (Figures 4c-d, g-
h, k-l, and Fig. S5d). On On $t-1$ days, a slight northward displacement of the low-pressure anomaly is associated with strong
northerly winds and positive air masses over Northern Canada, accompanied by a weakening of the westerly flow across the
selected grid box (Figures 4k and 5g). By the event day, the low-pressure system intensifies further, becoming more robust
and driving enhanced westerly flow with air masses extending west-northward (Figures 4l, 5h). Nevertheless, the average
temperature of the air masses three days before their arrival increases by 10.3°C on the day of the event, compared to a warming
by only 7.5°C for the trajectories initialized at $t-1$, which is due to the generally larger warming at higher latitudes, where the
air masses on the day of the event originate, associated with Arctic amplification (Figure 5p, Figs. S6d-f, and Figs. S7b and
725 d). As a result, the contribution of advective cooling is substantially reduced in future events relative to the historical period
($+2.8^{\circ}\text{C}$, Figure 6d). Vertical motion changes also show slightly enhanced subsidence at t (approximately 4-5 hPa in 3d; Figure
5l), which contributes to a modest increase in adiabatic warming ($+0.4^{\circ}\text{C}$) and further limits surface cooling. Diabatic cooling
is similarly weaker in the future climate, with a slightly greater reduction on day $t-1$ —particularly during the final 24 hours
(Figure 5t)—leading to an additional change of $+0.4^{\circ}\text{C}$. Overall, the dominant factor limiting future DTD T cooling ($+3.6^{\circ}\text{C}$)
730 is the reduced strength of cold air advection, likely associated with Arctic amplification (Fig. S7d), with smaller but reinforcing
contributions from enhanced adiabatic warming and reduced diabatic cooling (Figure 6d).

Deleted: -

Deleted:

Deleted: -

Deleted: dominates

Deleted: -

Deleted: -

Deleted: 4

Deleted: -

Deleted: -

Deleted: by

Deleted: -

Deleted: -

Deleted: -

Deleted: -

Deleted: 6

Formatted: English (US)

Formatted: English (US)

Formatted: Font: (Default) Times New Roman, Font color: Auto, English (US), Pattern: Clear

Formatted: Font: (Default) Times New Roman, Font color: Auto, English (US), Pattern: Clear

Formatted: Font: (Default) Times New Roman, Font color: Auto, English (US), Pattern: Clear

Deleted: A comparison of North American cooling events reveals that, while the diabatic cooling is similar between CESM-LE and ERA5, in CESM-LE, (see Figures 4d-f and 5l, in Part I)

Formatted: Font: (Default) Times New Roman, Font color: Auto, English (US), Pattern: Clear

Formatted: Font: (Default) Times New Roman, Font color: Auto, English (US), Pattern: Clear

Formatted: English (US)

Deleted: -

Deleted: -

Deleted: -

Deleted: 4

Deleted: On both days, a slight northward shift of the low-pressure anomaly is associated with (north-) westerly wind anomalies in the selected grid box (Figures 4k

Deleted: , l) and a westward shift of the trajectory origins (Figures 5g, h).

Deleted: -

Deleted: likely

Deleted: -

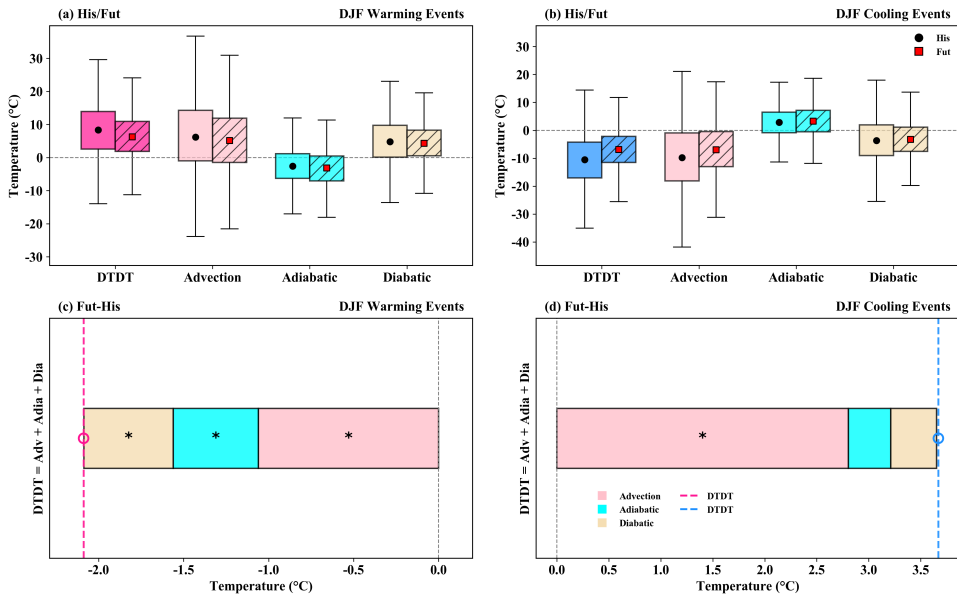
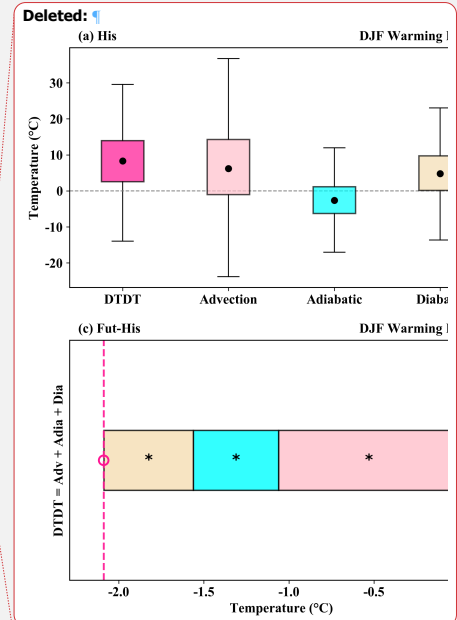


Figure 6. The contribution of the different physical processes (advection, adiabatic and diabatic temperature change) over North America during December–February (DJF) to genesis of DTDT, (a, c) warming and (b, d) cooling events during historical/future climate (a–b, box plots) and projected change (c–d, stacked plots) according to Eq. (2), which refers to a 3d₀ time scale. The box spans the 25th and 75th percentiles of the trajectory data; the black dot/red square inside the box gives the mean of the related quantities in the historical/future climate, and the whiskers indicate 1.5 times the interquartile range in panels (a) and (b). The dotted lines in the stacked plots in panels (c) and (d) show the mean future change for DTDT warming and cooling events, respectively, and coloured bars indicate the contributions of the individual processes. Circle and * symbols mark future change distributions for which the ensemble means differences exceed the 95% confidence threshold based on a t_{τ} test.

The CESM_{LE} future projections suggest that extreme DTDT changes will also weaken during JJA in some extratropical regions, including eastern and western North America, Northeastern Asia, Greenland, and Chile. Regarding the underlying processes, the results differ from those of extreme DJF events, with only the advective component weakening, contributing to this reduction (Fig. S13–16). Additionally, changes in diabatic (Fig. S16) or adiabatic processes may also occur. As an example, a grid box in western North America is examined in detail in the following section (Figures 7–9).



Formatted: Justified

Formatted: Font: Bold, Font color: Auto, English (UK)

Deleted: -

Deleted: -

Formatted

[... [25]

Formatted

[... [26]

Deleted: future

Deleted: -

Deleted: -

Formatted: English (UK)

Formatted

[... [27]

Formatted

[... [28]

Deleted: mean...ans differences exceed the 95% confidence threshold based on a Student's ...-

[... [29]

Formatted: Font: Not Bold

Deleted: ...LE future projections suggest that extreme DTDT changes will also weaken during JJA in some extratropical regions, including eastern and western North America, Northeastern Asia, Greenland, and Chile. Regarding the underlying processes, (... [30]

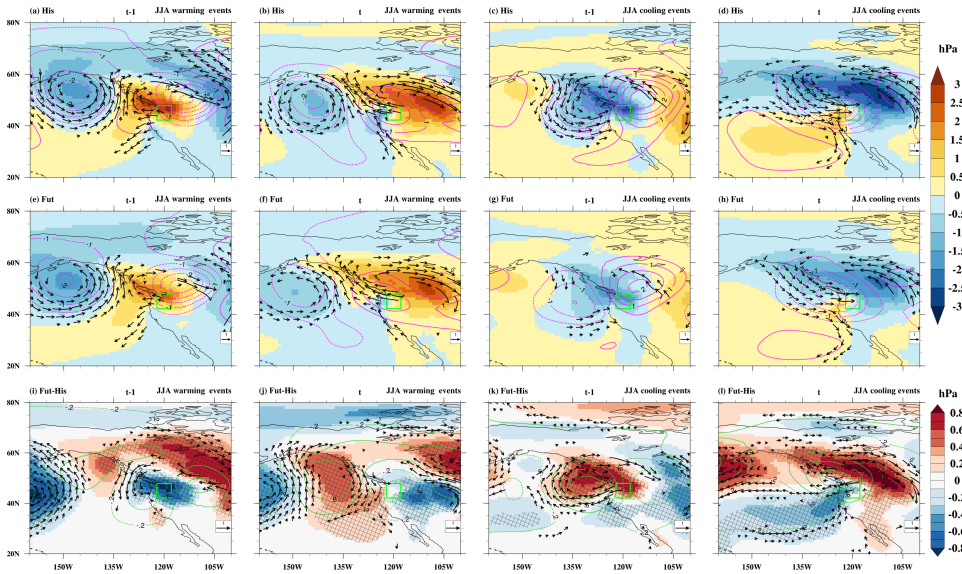


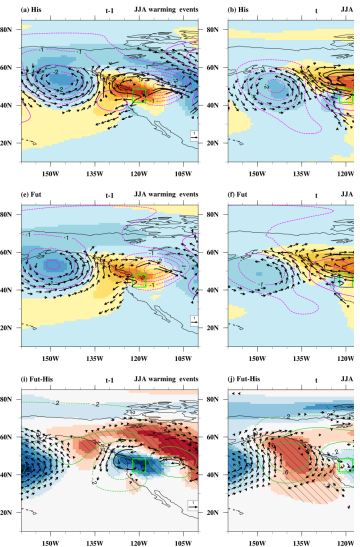
Figure 7. Composite of sea level pressure anomalies (hPa, color shading), wind anomalies at 850 hPa (m s^{-1} , vectors), and geopotential height anomalies at 500 hPa (gpm, magenta and darkgreen contours) relative to the seasonal mean on the (a, e, i, c, g, k) previous day ($t-1$) and (b, f, j, d, h, l) event day (t) of the warming (a, b, e, f and i, j) and cooling (c, d, g, h and k, l) events during June–August (JJA) in (a, d) historical climate (His), (e, h) future climate (Fut), and (i, l) projected changes (Fut–His) at a selected grid box in western North America (green box). Note that, in (a–h), wind vector anomalies $> 1 \text{ m s}^{-1}$ and in (i, j), wind vector difference anomalies $\geq 0.5 \text{ m s}^{-1}$ are plotted. The dotted and bold contours indicate negative and positive geopotential height anomalies, respectively. Additionally, the **cross-hatching** area shows where the ensemble mean of sea level pressure differences exceeds the 95% confidence threshold based on a t -test.

820

825

In the historical climate simulations, DTDI warming events are typically associated with a positive SLP anomaly near the selected grid box at $t-1$, but with a cyclonic 500 hPa anomaly with a maximum to the east (Figure 7a). Winds near the grid box are weak, and air masses originate in the vicinity, mostly over the continent (Figure 8a). By day t , the cyclonic anomaly at 500 hPa is replaced by a mature anticyclonic anomaly that began developing along the west coast on day $t-1$ (Figure 7b). This transition is associated with the accumulation of warmer air masses over the continent beneath an amplified upper-level ridge (Fig. S13a and Figure 8b). Nevertheless, wind changes near the grid box between $t-1$ and t are small, and air masses have nearly identical source regions (Figures 8a–b) and source temperatures (Figure 8m). Accordingly, the contribution of advection to the warming is small and even slightly negative (-0.4°C); however, there is significant variability between individual events (Figure 9a). The warming is thus driven by adiabatic and diabatic processes during the three days of air mass

830



Deleted:

Deleted: -

Formatted

... [31]

Deleted: -..., e-... and i--

... [33]

Deleted: -..., g-... and k-... events during June-

... [34]

Deleted: -

Formatted

... [32]

Formatted: Font: Not Bold

Formatted: Font: Not Bold

Deleted: -

Deleted: -... projected future... changes (Fut-

... [35]

Formatted: Font: Not Bold

Formatted: Font: Not Bold

Deleted: -

Deleted: -

Formatted: Font: Not Bold

Formatted: Font: Not Bold

Deleted: hatched ...rea shows where the ensemble mean of sea level pressure differences exceeds the 95% confidence thres...

... [36]

Deleted: anomaly at ...00 hPa anomaly with a maximum to the east (Figure 7a). Winds near the grid box are weak, and air t...

... [37]

transport, with increased adiabatic warming due to stronger subsidence within the anticyclonic circulation anomaly at t compared to $t-1$, contributing $+2.4^{\circ}\text{C}$ (Figures 8i, m, 9a). Near the surface, the descent weakens, allowing substantial diabatic warming likely linked to surface sensible heat fluxes, which further elevate surface temperatures (Figure 8q) and contribute approximately $+3.4^{\circ}\text{C}$ to the temperature change. Overall, warm advection plays a negligible role for DTDT warming events during the historical period, which are instead driven by increasing descent and diabatic heating (Figure 9a). However, note that the roles of advection and adiabatic processes in CESM-LE are reversed, with larger magnitudes differing from those in the ERA5 (Fig. S5c in Part 1). Nevertheless, according to ERA5, diabatic warming is the primary contributor to DTDT warming events, with a magnitude nearly equal to that in CESM-LE.

895 In the future climate scenario, the synoptic pattern resembles that of the historical climate, albeit with subtle changes. DTDT warming events are linked to smaller positive SLP anomalies and a weakened anticyclonic circulation over the West Coast at $t-1$ (Figures 7e, i). This goes along with a further reduction in the transport of oceanic air masses and increases the presence of northerly and localised air masses near the target grid point at $t-1$ (Figure 8e). By day t , the anticyclonic anomaly centred over the grid point is also weaker (Figure 7f, j) and air mass origins shift slightly northward (Figure 8f). Although there is a slight shift towards warm air advection (Figures 8m, n), contributing approximately $+0.7^{\circ}\text{C}$ to the projected change in DTDT magnitude, it does not compensate for the overall reduction (Figure 9c). The primary driver of the projected decline in DTDT warming is a significant decrease in adiabatic warming (-1.2°C) due to a smaller mean descent of air masses (by -11 hPa) particularly on the day of the event (Figures 8i, j), which is linked to a weakening of the anticyclonic anomaly at 500 hPa described above (see again Figure 7j, Fig. S13c). Surface diabatic heating plays a secondary role. Since changes in heating are slightly greater on day $t-1$ than on day t , it contributes an additional -0.3°C to the overall reduction (Figure 8r). Thus, the decline in adiabatic warming, combined with a modest reduction in surface diabatic heating, is the key factor decreasing the magnitude of DTDT warming events under future climate conditions (Figure 9c). However, when considering only the last day before arrival, the changes in diabatic heating are the main factor weakening the DTDT warming (by -0.9°C), while adiabatic warming changes are weaker and of opposite sign ($+0.3^{\circ}\text{C}$). This suggests that the process decomposition of DTDT warming events over western North America depends on the temporal limits of the analysis.

Deleted: -

Deleted: underestimated and

Deleted: compared to those

Deleted: reanalysis

Deleted: data

Deleted: part I

Deleted: Nevertheless, according to ERA5, diabatic warming is the largest contribution to DTDT warming events.

Deleted: -

Deleted: -

Deleted: southward

Deleted: projected future

Deleted: 7

960 During historical DTDT cooling events, an anticyclonic circulation anomaly at 500 hPa over and to the east of the selected grid box at day $t-1$ shifts further eastward and is replaced by an eastward-moving cyclonic anomaly from the Pacific Ocean on the day of the event (Figure 7c-d). This is accompanied by an eastward shift of a negative SLP anomaly and stronger westerly winds on the southern flank of the cyclonic anomaly reaching the grid box on day t , such that the density distribution of air masses extends further into the western Pacific region compared to $t-1$ (Figures 8c-d). As a result, a slight shift towards cold air advection leads to an average temperature drop of -1.6°C (Figures 8o, 9b). This advective cooling is partly offset by a modest increase in adiabatic warming ($+1^{\circ}\text{C}$) due to stronger air mass descent on the day of the event (Figures 8k, o).

965 However, the main factor driving the DTDT decrease is reduced diabatic heating near the surface on day t relative to $t-1$ (Figure 8s), mainly on the last day before the trajectories arrive (Figure 9b), with a mean contribution of -5.5°C . These processes are the same in ERA5, but CESM-LE overestimates adiabatic and diabatic processes and underestimates advection in its representation of DTDT cooling events (see Fig. S5d in Part 1).

970 In projected DTDT cooling events, the configuration of circulation anomalies remains similar to present-day, but their magnitude significantly weakens (Figures 7g-h, k-l, and S13d). At $t-1$, air masses predominantly originate from the north with a slight oceanic extension, whereas by day t they shift toward the continent, accompanied by a marked reduction in oceanic masses due to weakened westerly winds on the southern flank of the cyclonic anomaly (Figures 8g, h, and Fig. S13d). Together, this leads to a future reduction in the temperature difference between $t-1$ and t at the air mass origin (Figure 8o, p), thereby reducing the contribution of cold air advection to the DTDT cooling by approximately $+0.4^{\circ}\text{C}$ (Figure 9d). The cooling is further suppressed by increased adiabatic warming ($+0.7^{\circ}\text{C}$), linked to stronger mean ascent (by 6 hPa) at day t (Figures 8k, o). Near the surface, diabatic cooling is projected to increase slightly by -0.3°C in the future (Figure 8s). Therefore, future reductions in DTDT cooling events are mainly driven by reduced advection and further increases in adiabatic warming, with changes in diabatic cooling playing only a minor role (Figure 9d).

- Deleted:** -
- Deleted:** *1 day*
- Deleted:** -
- Formatted:** Font: Italic
- Deleted:** -
- Deleted:** -
- Deleted:** -
- Deleted:** -
- Deleted:** is
- Deleted:** pattern aligns with ERA5 reanalysis results, lending confidence to the
- Deleted:** representation
- Deleted:** of
- Deleted:** Part I
- Deleted:** future
- Deleted:** stay
- Deleted:** -
- Deleted:** -
- Deleted:** -
- Deleted:** 7
- Formatted:** Not Highlight
- Deleted:**). Air mass origins shift towards the continent at $t-1$, but northward and towards the ocean, with a reduction continental airmass on day t (Figures 8g, h)
- Formatted:** Not Highlight
- Deleted:** -
- Formatted:** Font: Italic
- Deleted:** slightly
- Deleted:** in the future (
- Deleted:** -
- Deleted:** ,

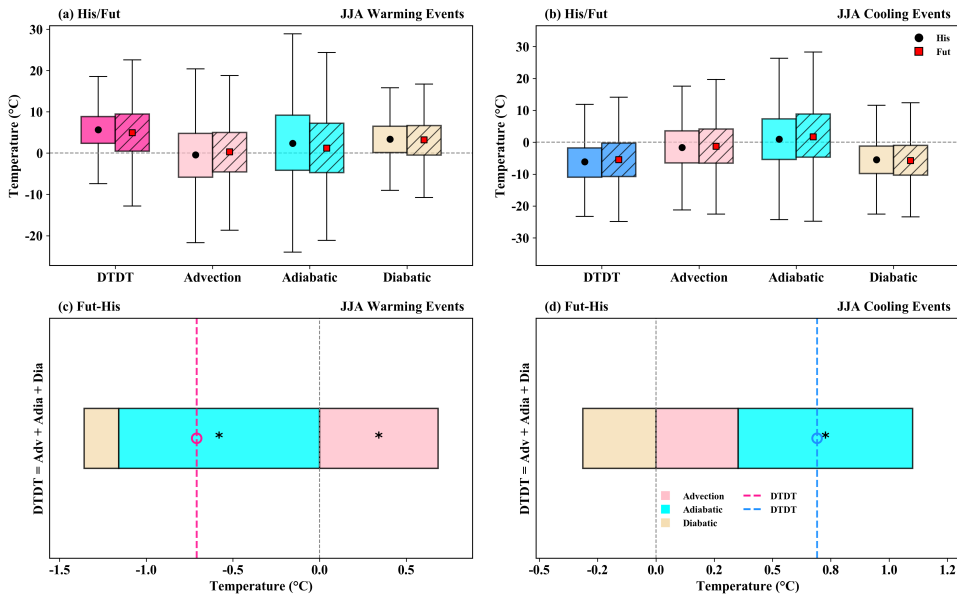
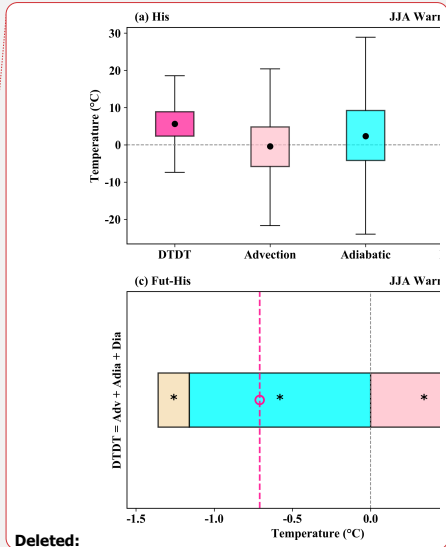


Figure 9. The contribution of the different physical processes (advection, adiabatic and diabatic temperature change) over western North America during June–August (JJA) to the genesis of DTD T (a, c) warming and (b, d) cooling events during historical/future climate (a–b, box plots) and projected change (c–d, stacked plots) according to Eq. (2), which refers to a 3d–time scale. The box spans the 25th and 75th percentiles of the trajectory data; the black dot/red square inside the box gives the mean of the related quantities in the historical/future climate, and the whiskers indicate 1.5 times the interquartile range in panels (a) and (b). The dotted lines in the stacked plots in panels (c) and (d) show the mean future change for DTD T warming and cooling events, respectively, and coloured bars indicate the contributions of the individual processes. Circle and * symbols mark future change distributions for which the ensemble means differences exceed the 95% confidence threshold based on a t -test.

3.2.2 Projected intensification of extreme DTD T changes

During DJF, many tropical regions (Amazon, southern Africa, and Southeast Asia) are projected to experience an increase in extreme DTD T changes compared to the historical climate. To investigate the mechanisms behind extreme DTD T changes, we focus on a specific location in tropical South America (Figures 10e–12; see Figs. S17–18 for another location in tropical Southern Africa).

In the CESM historical simulation, air masses at $t-3d$ cluster around the selected target grid box, indicating that local conditions mainly drive DTD T changes (Figure 10a–d), similar to the ERA5 analysis (see Figure 9a–d in Part 1). During warming events, the temperature and pressure evolution along the backward trajectories is very similar for trajectories initialised at $t-1$ and t



Deleted:

Deleted: ... August (JJA) to the genesis of DTD T (a, c) warming and (b, d) cooling events during historical/future ... climate (a–..., box plots) and projected future...change (c–..., stacked plots) according to Eq. (2), which refers to a 3d–...time scale. The box spans the 25th and 75th percentiles of the trajectory data; the black dot/red square inside the box gives the mean of the related quantities in the historical/future ... climate, and the whiskers indicate 1.5 times the interquartile range in panels (a) and (b). The dotted lines in the stacked plots in panels (c) and (d) show the mean future change for DTD T warming and cooling events, respectively, and coloured bars indicate the contributions of the individual processes. Circle and * symbols mark future change distributions for which the ensemble mean...ens differences exceed the 95% confidence threshold based on a Student's ...-...test. ¶

Deleted: future

Formatted: Heading 2

Deleted: ... 12; see Ff...gs. ures ...170–...18S11

Deleted: ...3d cluster around the selected target grid box, indicating that local conditions mainly drive DTD T changes (Figure 10a–...d), similar to the ERA5 analysis (see Figure 9a–...d in Part 1...art 1). During warming events, the temperature and pressure evolution along the backward trajectories is very similar for trajectories initialised at $t-$

between 3 and 1 days before reaching the target location (Figures 10i and m), while diabatic heating within the last 24 hours plays a significant role for the DTDT increase (Figure 10q). Therefore, we analyse the physical processes on a one-day time scale (Figure 11a), in contrast to the 3-day analysis presented above for the extratropics. Composite precipitation and cloud cover are further analysed in Figure 12 to explore these local diabatic effects. On day $t-1$, significant precipitation ($5-8 \text{ mm d}^{-1}$) and high cloud cover ($80-90 \%$) reduce solar radiation and thus diabatic heating, leading to lower temperatures. Conversely, on day t , decreased precipitation ($\leq 3 \text{ mm d}^{-1}$) and less cloud cover ($70-80 \%$) enhance diabatic heating, contributing to higher temperatures (Figures 10m, 12b). This shift from wet and cloudy to dry and less cloudy conditions highlights the role of albedo changes and solar heating in driving a $+2^\circ\text{C}$ increase over 1d, with enhanced diabatic heating ($+2.2^\circ\text{C}$; Figure 11a). The magnitudes of DTDT warming events in ERA5 and CESM-LE are nearly identical, reflecting a similar scale of diabatic heating but underestimation in the adiabatic process (see also Figure 9k in Part 1 and Figure 11a).

The localised patterns persist during future DTDT warming events, with high air particle densities at -3d continuing to cluster in the grid box and towards its northeast (reduced in the South) in both days. (Figures 10e-f). Thus, changes in remote advection and adiabatic warming play only a minor role in future DTDT changes (Figures 10j, n and 11c). The projected warming is primarily driven by diabatic heating (nearly $+1^\circ\text{C}$) near the surface over the last 24 hours, emphasising the enhanced role of radiative heating (Figures 10r and 11c). This finding is further supported by a significant increase in precipitation and cloud cover on day $t-1$, which, however, subsequently decreases on day t , contributing to the intensified DTDT warming in the future climate (Figures 12i-j). Also, for tropical Southern Africa (Fig. S17c) and Southeast Asia (not shown), the intensification of DTDT warming events is mainly driven by diabatic heating.

Deleted: -

Deleted: -

Deleted: -

Deleted: -

Deleted: -

Deleted: temperature

Deleted: driven by

Deleted: ,

Deleted: -

Deleted: part I

Deleted: The localised patterns persist during future DTDT warming events, with high air particle densities at -3d continuing to cluster around the grid box and towards its east (reduced in the west) for day $t-1$. For day t , they are distributed even closer to the grid cell (reduced in the south) compared to the historical climate

Deleted: -

Deleted: -

Deleted: -

Deleted: 0

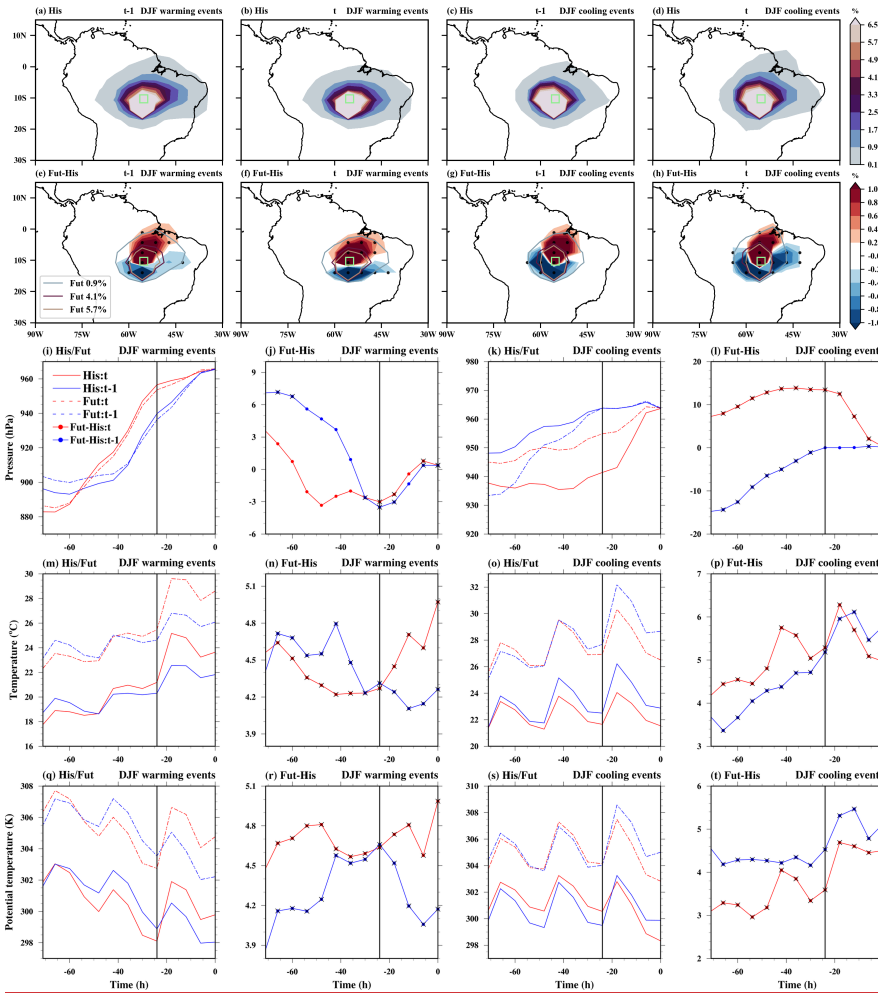


Figure 10. The spatial distribution of trajectory density initiated on the previous day ($t-1$) and the event day (t) is depicted for both December–February (DJF) warming and cooling events over tropical South America (green box). Color shading shows the air mass density (%) during the 3d before arriving at the target grid box for (a–d) historical climate and (e–h) projected change. In (e–h), stippling areas indicate where the ensemble mean of density differences exceeds the 95% confidence threshold based on a t -test. The colour contours the outline of the different future–trajectory density. The mean Lagrangian evolution of distinct physical parameters (pressure, temperature, potential temperature) is shown along the air mass trajectories initialised on the previous and event days for historical/future extreme events

Deleted: [47]

- Deleted: -
- Formatted: Font: Not Bold
- Deleted: -
- Deleted: -
- Deleted: -
- Deleted: future
- Deleted: -
- Formatted: Font: Not Bold
- Formatted: Font: Not Bold
- Formatted: Font: Not Bold
- Deleted: stippling indicates areas where $\geq 80\%$ of the ensemble members agree on the sign of change

(1st and 3rd columns) and for projected changes in extremes (2nd and 4th columns). Additionally, bold circles with crosses show where the ensemble mean differences at each timestep exceed the 95% confidence threshold based on a t -test.

Also, for the historical DTD cooling events, the distribution of air masses on both days is concentrated around the grid box, with remote advection and adiabatic heating playing little role for the temperature decrease (Figures 10c-d, k, o, s, 11b). These events are primarily driven by local diabatic effects near the surface in the 24 hours preceding the arrival of the air masses at the target location, with magnitudes comparable to those in the ERA5 reanalysis, but biases in the adiabatic process (see Figure 9l in Part 1). Similar to DTD warming events, on day $t-1$, precipitation (8–10 mm d⁻¹) and cloud cover (70–80 %) are smaller, leading to increased diabatic heating and higher temperatures, compared to the larger precipitation (>10 mm d⁻¹) and cloud cover (80–90%) on day t , which result in decreased diabatic heating and lower temperatures (Figures 11b and 12c-d). This transition from dry, less cloudy conditions to wet, cloudy conditions highlights the significant role of changes in albedo and solar heating in driving surface diabatic cooling.

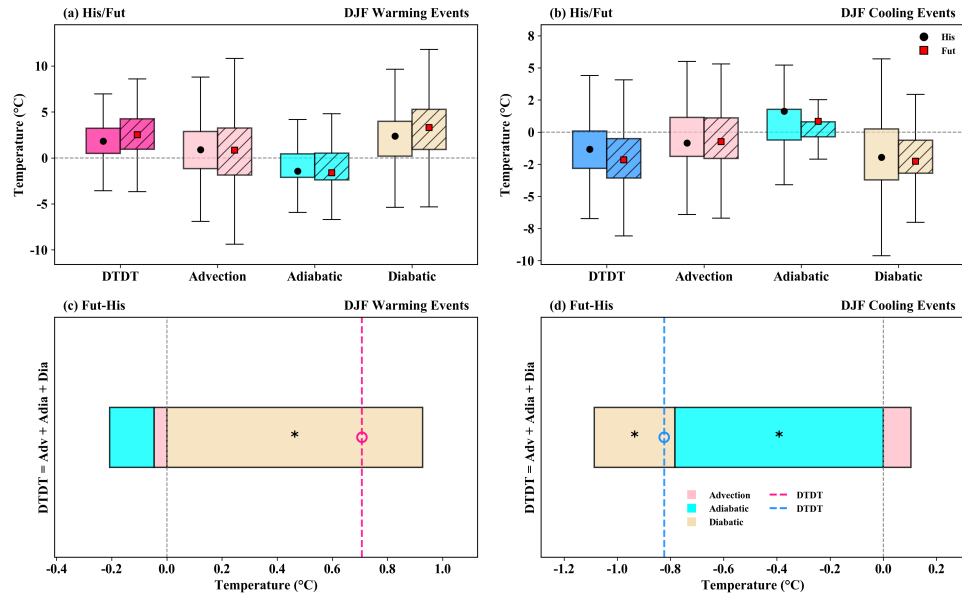


Figure 11. The contribution of the different physical processes (advection, adiabatic and diabatic temperature change) over tropical South America during December–February (DJF) to the genesis of DTD DTD (a, c) warming and (b, d) cooling events during historical/future climate (a–b, box plots) and projected change (c–d, stacked plots) according to Eq. (2), which refers to a 1d-time scale. The box spans the 25th and 75th percentiles of the trajectory data; the black dot/red square inside the box gives the mean of the related quantities in the historical/future climate, and the whiskers indicate 1.5 times the interquartile range in panels (a) and (b). The dotted lines in the stacked

Deleted: projected future

Formatted: Font: Not Bold

Formatted: Font: Not Bold

Deleted: Student's ...-

... [48]

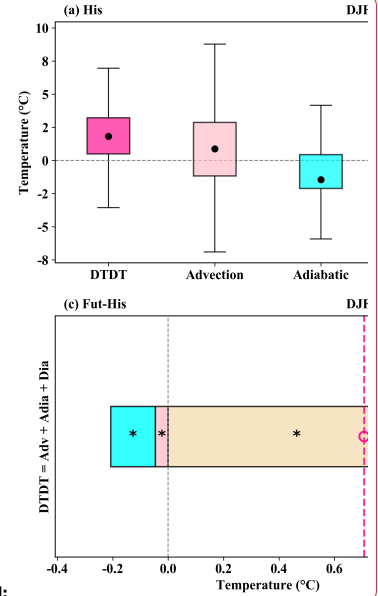
Formatted: Font: Not Bold

Deleted: ...d, k, o, s, 11b). These events are primarily driven by local diabatic effects near the surface in the 24 hours preceding the arrival of the air masses' arrival...at the target location, with magnitudes comparable to those of...n the ERA5 reanalysis, but biases in the adiabatic process (see Figure 9l in Part 1...art 1). Similar to DTD warming events, on day t -

... [49]

Deleted: -

Deleted: ...90%) on day t , which result in decreased diabatic heating and lower temperatures (Figures 11b and 12c-...d). This transition from dry, less cloudy conditions to wet, cloudy conditions... highlights...ighlights the significant role of changes in albedo and solar heating in driving surface diabatic cooling. (... [50]



Deleted:

Deleted: ... February (DJF) to the genesis of DTD DTD (a, c) warming and (b, d) cooling events during historical/future climate (a–...), box plots) and projected future ...change (c–...d, stacked plots) according to Eq. (2), which refers to a 1d-...time scale. The box spans the 25th and 75th percentiles of the trajectory data; the black dot/red square inside the box gives the mean of the related quantities in the historical/future

... [51]

plots in panels (c) and (d) show the mean future change for DTD cooling events, respectively, and coloured bars indicate the contributions of the individual processes. Circle and * symbols mark future change distributions for which the ensemble mean differences exceed the 95% confidence threshold based on a t_{-1} test.

In future DTD cooling events, local effects are projected to remain dominant, with increased air particle densities around and to the northeast of the grid box (reduced in the Southeast) compared to the historical climate (Figures 10g-h). While the contributions of changes in advection to the future intensification of DTD cooling are small, a reversal in the role of adiabatic warming is the primary factor for this intensification (Figure 11d). In contrast to the historical climate, in which a stronger descent and adiabatic warming on day t compared to $t-1$ slightly offsets the diabatically-driven cooling (Figures 10k, 11b), in the future, the ascent and adiabatic warming are projected to weaken on day t , leading to increased cooling (Figures 10l, p). In addition, an intensification of diabatic cooling (Figures 10t, 11d) associated with a marked decline in precipitation and cloud cover on day $t-1$, followed by an increase on day t (Figures 12k-l), further enhances DTD cooling. A consistent pattern is also evident in Southeast Asia (not shown). A synergy between adiabatic and diabatic processes, albeit with a larger contribution from diabatic changes, leads to future intensification of DTD cooling events over tropical Southern Africa (Fig. S17d).

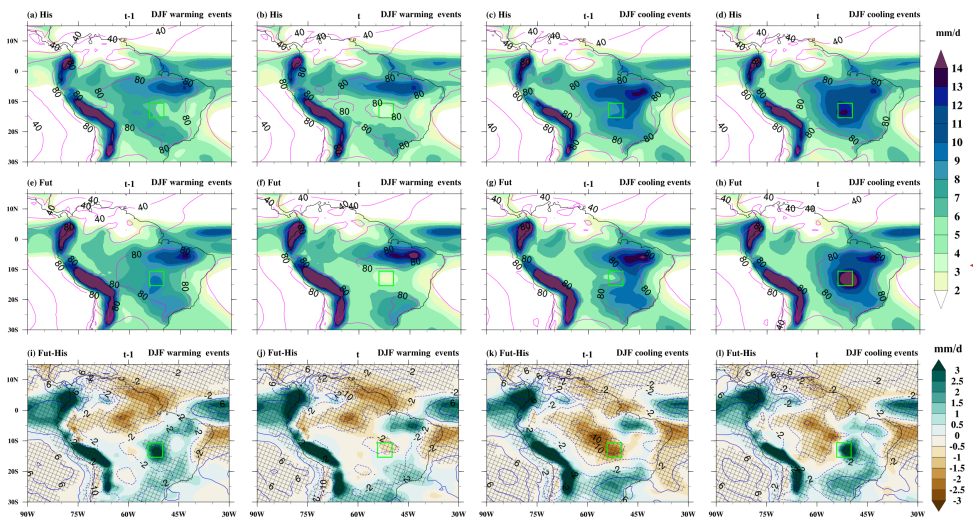


Figure 12. Composite of absolute total precipitation (mm d^{-1} , colour shading) and total cloud cover (%; magenta and blue contours) on the previous ($t-1$) and event (t) days of warming and cooling events during December-February (DJF) over South America. The top panel displays ensemble means for the (a-d) historical climate (His), (e-h) future climate (Fut), and (i-l) projected change (Fut-His). The green box represents the study grid box, and the cross-hatching area in (i-l) indicates that the ensemble mean of the total precipitation differences exceeds the 95% confidence threshold based on a t_{-1} test. The green and brown shading illustrate increases and decreases in total precipitation, respectively, while the magenta and blue bold and dotted contours represent increases and decreases in total cloud cover (in Figure i-l).

Deleted: Student's
Deleted: -

Deleted: southwest
Deleted: north
Deleted: -

Deleted: -
Deleted: -

Deleted: -
Deleted: -

Deleted:
Deleted: 0

Deleted: 1
Formatted

Formatted: Font: Not Bold

Deleted: -

Deleted: -

Deleted: -

Deleted: -

Deleted: projected future

Deleted: -

Deleted: ed

Deleted: Student's

Deleted: -

Deleted: -

During JJA, some sub-tropical and mid-latitude regions, such as the Sahel, parts of Europe, Southern Asia, Central America, and the Amazon, are projected to experience an increase in extreme DTD changes relative to the historical climate. To study the underlying atmospheric circulation and physical processes, we select a grid box over central Europe (Figures 13-15). Further examples for locations in the subtropics (Figs. S19-21) and midlatitudes (Figs. S22-24) are shown in the supplement.

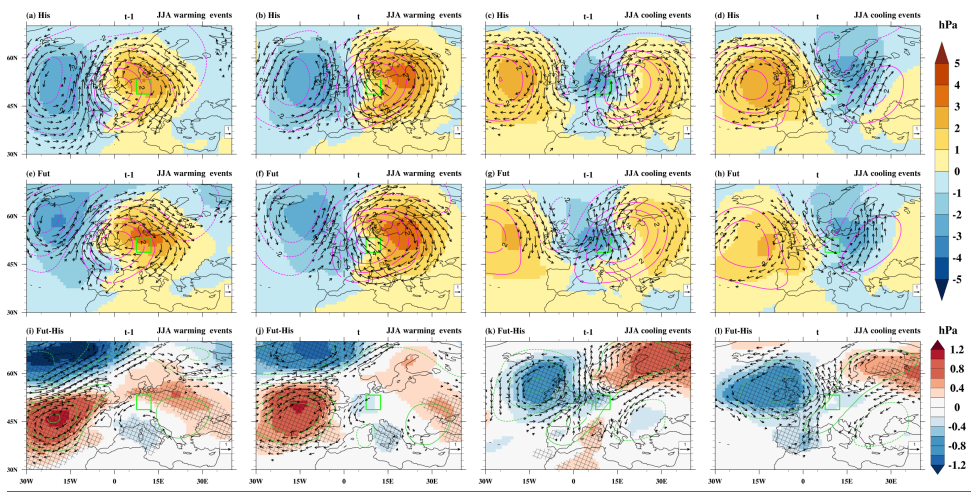


Figure 13. Composite of sea level pressure anomalies (hPa, color shading), wind anomalies at 850 hPa (m s^{-1} , vectors), and geopotential height anomalies at 500 hPa (gpm, magenta and darkgreen contours) relative to the seasonal mean on the (a, e, i, c, g, k) previous day ($t-1$) and (b, f, j, d, h, l) event day (t) of the warming (a, b, e, f and i, j) and cooling (c, d, g, h and k, l) events during June-August (JJA) in (a, d) historical climate (His), (e, h) future climate (Fut), and (i, l) projected changes (Fut-His) at a selected grid box in central Europe (green box). Note that, in (a-h), wind vector anomalies $\geq 3 \text{ m s}^{-1}$ and in (i, l), wind vector difference anomalies $\geq 0.5 \text{ m s}^{-1}$ are plotted. The dotted and bold contours indicate negative and positive geopotential height anomalies, respectively. Additionally, the cross-hatching area shows where the ensemble mean of sea level pressure differences exceeds the 95% confidence threshold based on a t -test.

During JJA warming in central Europe in the historical CESM-LE simulations, a mature trough-ridge anomaly pattern shifts eastward from day $t-1$ to t (Fig. S19a; Figures 13a-b), bringing central Europe under the influence of southerly winds and warm continental air masses on the event day (Figures 14a-b), which aligns with the ERA5 synoptic pattern (see Figure 6a-c and Fig. S6a-b in Part 1). This transition enhances warm air advection (Figure 14m), which plays a crucial role in driving the temperature increase, resulting in an average temperature rise of $+3.2^\circ\text{C}$ (Figure 15a). In contrast, adiabatic warming makes a minor negative contribution, averaging -0.3°C , due to slightly more substantial subsidence on day $t-1$ than on day t (Figures

Formatted: Caption

Deleted: 1

Deleted: 13-15

Deleted: 3-

Deleted: 14

Deleted: 15-

Deleted: 16

Deleted: 1

... [54]

Formatted: English (UK)

Deleted: -

Formatted: Font: Not Bold, Italic

Deleted: -

Deleted: -

Deleted: -

Deleted: -

Deleted: -

Deleted: -

Deleted: -

Deleted: -

Deleted: -

Deleted: -

Deleted: future

Deleted: -

Deleted: -

Deleted: -

Deleted: ed

Deleted: Student's

Deleted: -

Deleted: -

Deleted: -

Deleted: -

Deleted: 2

Deleted: -

Deleted: -

Deleted: Part I

1295 14i, m). However, the effect of adiabatic warming varies considerably across individual events, shown by the bars and whiskers (Figure 15a). Enhanced diabatic heating contributes an average of +2.5°C to the DTDT increase, with a more pronounced rise in potential temperature on day t than on day $t-1$ (Figure 14q). Overall, warm air advection and diabatic heating are the primary contributors to DTDT warming events, with adiabatic warming playing a minor role in the historical climate (Figure 15a). A quantitative comparison reveals that CESM-LE indicates contributions from advection and diabatic heating similar to those of ERA5, but the adiabatic warming is slightly underestimated (see Figure 7k, Part 1).

1300 In general, the synoptic-scale flow pattern associated with future DTDT warming events resembles the historical pattern (Figures 13e, f). Notable differences are nonetheless evident upstream over the North Atlantic, where the low-pressure anomaly weakens in future projections (Fig. S19c). Concurrently, the adjacent continental ridge experiences a structural reorganisation: its southwestern branch weakens, while the northeastern branch slightly intensifies and shifts eastward at day t (Figures 13i–j). Collectively, these circulation changes reduce the inflow of southwesterly maritime air masses and shift toward continental sources, contributing to enhanced DTDT warming (Figures 14e–f, Fig. S19c). These subtle changes in circulation patterns result in a modest increase in warm air advection, contributing approximately +0.5°C to the DTDT change (Figure 15c). Meanwhile, vertical descent intensifies on day $t-1$ (by ~5 hPa) but diminishes notably on day t (by ~10 hPa), leading to a negative adiabatic warming contribution that offsets the DTDT increase by -1.1°C (Figures 14j, n). Conversely, diabatic heating increases on both days compared to the historical period, with a greater increase on day t (Figure 14r). This intensified diabatic heating adds +1.9°C to the DTDT change. Overall, the combined effect of slightly increased warm air advection and amplified diabatic heating—despite being partly offset by enhanced adiabatic warming—appears to be the main factor driving the projected intensification of DTDT warming events (Figure 15c). A similarly important role of diabatic heating intensification is also evident in future DTDT warming events over the selected subtropical regions of southern Asia and the Sahel (Figs. S20–21), as well as in Central America and northern Amazon (not shown). In contrast, changes in advection are more significant for events in southern South Africa, northern Asia, southern Australia (Figs. S22–24), and northern Europe (not shown).

1315

Deleted: θ

Deleted: -

Deleted: part 1

Deleted: -

Deleted: However, notable differences are evident, particularly upstream over the North Atlantic (Figures 13i, j), where the low-pressure anomaly weakens. Simultaneously, the adjoining ridge pattern at 500 hPa over the continent shifts slightly southeastward compared to the historical period. Together, these result in a decrease in the inflow of westerly, maritime air masses and a shift towards continental sources on both days involved in the DTDT warming (Figure 14e, f).

Deleted: -

Deleted: projected future

Deleted: 13-

Deleted: 14

Deleted:

Deleted: 15-

Deleted: 16

1320

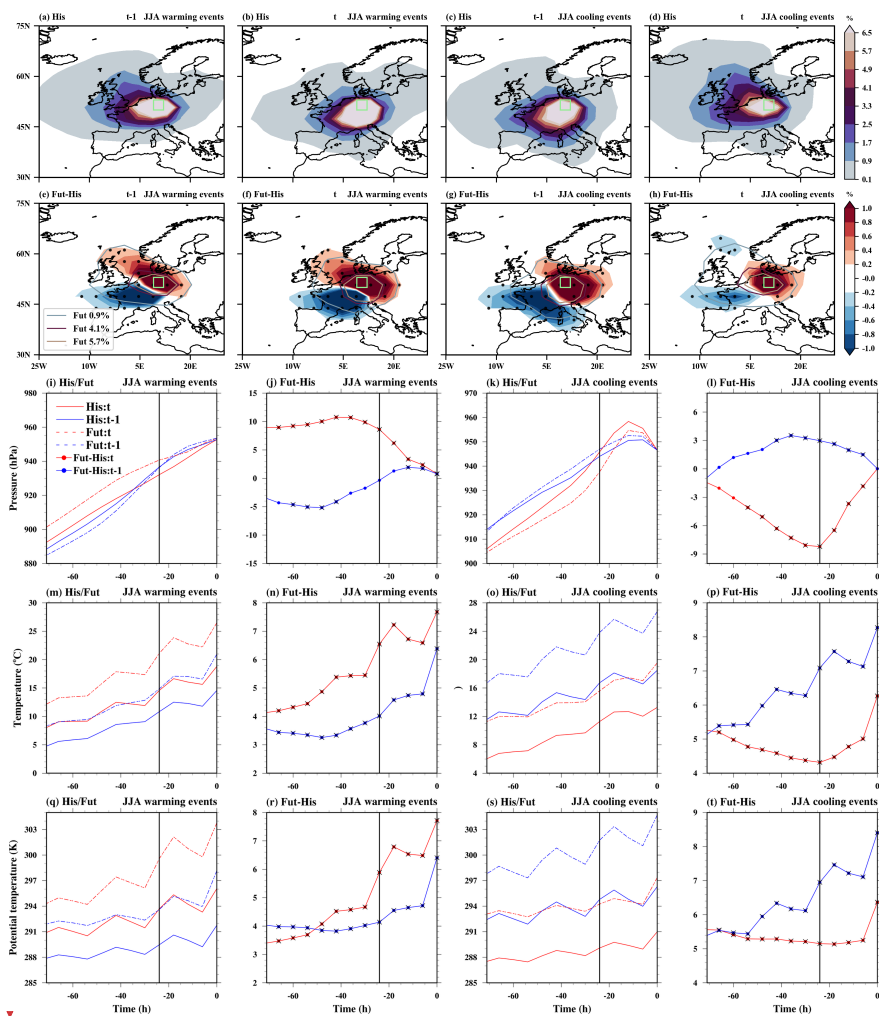
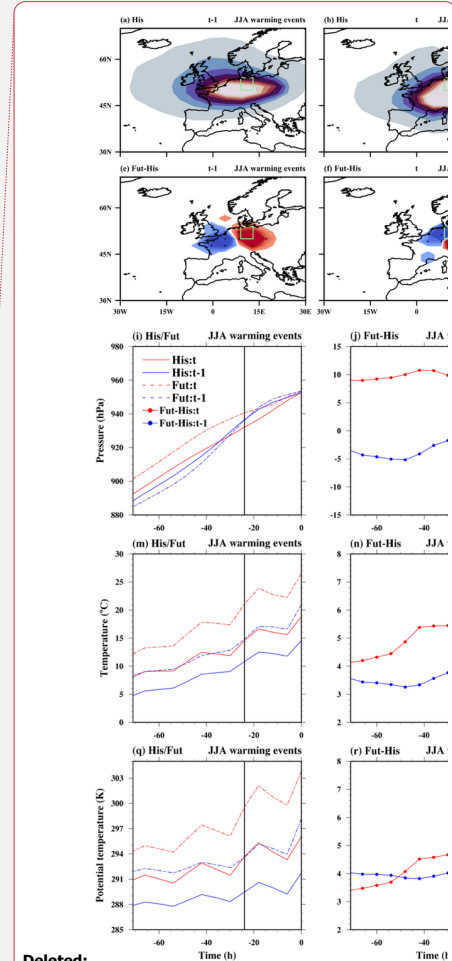


Figure 14. The spatial distribution of trajectory density initiated on the previous day ($t-1$) and the event day (t) is depicted for both June–August (JJA) warming and cooling events over central Europe (green box). Color shading shows the air mass density (%) during the 3d before arriving at the target grid box for (a–d) historical/future climate and (e–h) projected change. In (e–h), stippling areas indicate where the ensemble mean of density differences exceeds the 95% confidence threshold based on a t -test. The contours outline the 0.9%, 4.1%, and 5.7% levels of future trajectory density. The mean Lagrangian evolution of distinct physical parameters (pressure, temperature, and potential



Deleted:

Deleted: -

Deleted: -

Formatted

... [55]

Formatted

... [56]

Formatted

... [57]

Deleted: -

Deleted:

Deleted: -

Deleted: future

Deleted: -

Formatted: Font: Not Bold

Formatted: Font: Not Bold

Formatted: Font: Not Bold

Formatted: Font: Not Bold

Formatted

... [58]

Deleted: stippling indicates areas where $\geq 80\%$ of the ensemble members agree on the sign of change.

Formatted: English (UK)

temperature) is shown along the air mass trajectories initialised on the previous and event days for historical/future extreme events (**1st and 3rd columns**) and **projected** changes in extremes (**2nd and 4th columns**). Additionally, bold circles with crosses show where the ensemble mean differences at each timestep exceed the 95% confidence threshold based on a t -test.

During JJA cooling events in the historical climate, there is a transition from warm continental air masses to colder maritime air masses, coinciding with the development and eastward shift of a North Atlantic ridge (Figures 13c-d, 14c-d and Fig.S19b). This cold air advection causes an average decline in surface temperature of -5.5°C (Figures 14o, 15b). The cooling is partly offset by a modest increase in adiabatic warming ($\sim 0.7^{\circ}\text{C}$), driven by stronger descent of air masses on day t (Figures 14k, o). Additionally, reduced diabatic heating contributes a further temperature drop of -0.5°C (Figure 14s). Overall, strong cold air advection and slightly reduced diabatic heating are the main drivers of DTD cooling events over central Europe under historical conditions (Figure 15b), which also agrees with the ERA5 reanalysis (see Figure 71 in Part 1). In the CESM_r-LE, the contributions from advection and adiabatic warming are somewhat **smaller**, but the diabatic contribution is similar to that in ERA5.

For projected DTD cooling events, on both days, the synoptic atmospheric circulation over the continent remains largely similar to that in the historical climate (Figures 13c-d, g-h). **Nevertheless, notable changes are expected along the North Atlantic ridge. The high-pressure anomaly weakens at both the surface and 500 hPa (Fig. S19d), and an eastward shift of the ridge becomes evident at day t (Figures 13k-l).** Regarding air-mass origins, a reduction in southwesterly maritime air masses and a concurrent increase in continental northeasterly air masses are evident, both more pronounced on day $t-1$ than on day t (Figures 13k-l, and 14g-h). Together, this slightly reduces the contribution of horizontal temperature advection to the DTD cooling ($+0.3^{\circ}\text{C}$). **Projected** changes in adiabatic warming are negligible (Fig. 14l, 15d), such that changes in diabatic heating are the primary contributor to the future DTD cooling (-2.2°C) intensification, which results from a much stronger intensification of the diabatic heating of air masses on day $t-1$ compared to day t (Figures 14t, 15d). Changes in diabatic heating are also the main driver of the future intensification of DTD cooling over Southern Asia, the Sahel, Northern Asia (Figs. S20-21, S23), Central America, the northern Amazon, and Northern Europe (not shown). **At the same time, either advection or all processes contribute more equally to events over southern South Africa, northern Asia, and Australia (Fig. S23-24).**

Formatted: Font: Bold

Formatted: Font: Bold, Not Superscript/ Subscript

Formatted: Font: Bold

Deleted: projected future

Formatted: Font: Bold, Not Superscript/ Subscript

Formatted: Font: Bold

Formatted: Font: Bold

Formatted: Font: Bold, Not Superscript/ Subscript

Formatted: Font: Bold

Formatted: Font: Bold, Not Superscript/ Subscript

Formatted: Font: Bold

Deleted: Student's

Deleted: -

Formatted: Font: Not Bold

Deleted: -

Deleted: -

Deleted: 2

Deleted: Part I

Deleted: -

Deleted: larger

Deleted: future

Deleted: -

Deleted: -

Deleted: , and Fig. S12d

Deleted: However, changes are projected over the North Atlantic, where the intensity of the high-pressure anomalies weakens at both the surface and 500 hPa (Figure 13k-l). Regarding the air mass origin, this is associated with an increase in westerly sources on both days, a reduction in southerly inflow at day $t-1$, and a reduction in northeasterly sources on day t (Figure 14g-h).

Deleted: Projected future

Deleted:

Deleted: (-2.2°C)

Deleted: -

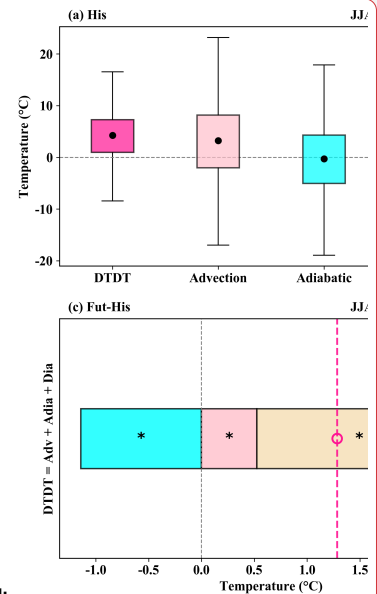
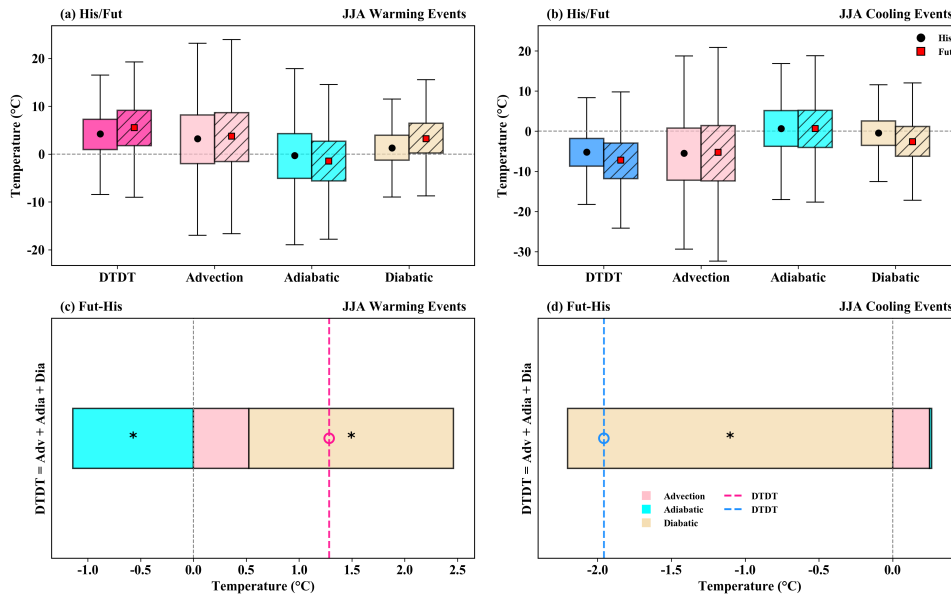
Deleted: 13-

Deleted: 14

Deleted: 16

Deleted: as well as

Deleted: At the same time, all processes contribute more equally to events over southern South Africa (Fig. S15).



425 **Figure 15.** The contribution of the different physical processes (advection, adiabatic and diabatic temperature change) over central Europe during June–August (JJA) to the genesis of DTD T (a, c) warming and (b, d) cooling events during historical/future climate (a, b) box plots) and projected change (c, d, stacked plots) according to Eq. (2), which refers to a 3d_y time scale. The box spans the 25th and 75th percentiles of the trajectory data; the black dot/red square inside the box gives the mean of the related quantities in the historical/future climate, and the whiskers indicate 1.5 times the interquartile range in panels (a) and (b). The dotted lines in the stacked plots in panels (c) and (d) show the mean future change for DTD T warming and cooling events, respectively, and coloured bars indicate the contributions of the individual processes. Circle and * symbols mark future change distributions for which the ensemble means differences exceed the 95% confidence threshold based on a *t*-test.

4. Discussion and Summary

435 This study has examined historical patterns and projected changes in extreme DTD T variations and their underlying physical processes based on the CESM_rLE, a large single-model ensemble designed to understand Earth system variability and global change (Kay et al., 2015). Our results from the CESM_rLE in the historical climate indicate that DTD T variations and extremes are more pronounced in the extratropics than in the tropics during both DJF and JJA, consistent with the ERA5 reanalysis (see also Figures 1–3 in Part 1). A comparison of CESM_rLE and ERA5 reanalysis results reveals notable regional differences in magnitude, particularly an overestimation in mid-to-high latitudes and Southeast Asia during DJF, and in some subtropical areas during JJA. The differences in daily standard deviations align with patterns observed in other models from the CMIP5

Deleted:

Formatted: English (UK)

Deleted: -

Deleted:

Deleted: -

Formatted

... [59]

Formatted

... [60]

Formatted

... [61]

Deleted: future

Deleted: -

Deleted: -

Formatted

... [62]

Formatted

... [63]

Formatted

... [64]

Deleted: mean...ans differences exceed the 95% confidence threshold based on a Student's ...-

... [65]

Formatted

... [66]

Formatted: Heading 2

Deleted: projected future...rojected changes in extreme DTD T variations and their underlying physical processes based on

... [67]

Deleted: -...LE in the historical climate indicate that DTD T variations and extremes are more pronounced in the extratrop

... [68]

and CMIP6 initiatives (Bathiany et al., 2018; Giorgi & Raffaele, 2022). The larger magnitude of σ_{DTDT} in CESM-LE is due to both higher daily standard deviations and lower autocorrelation compared to ERA5, and vice versa for the smaller magnitude of σ_{DTDT} , particularly in the tropics and subtropics (Fig. S1). The overestimation of extremes, primarily in the extratropics, in DJF is driven often by diabatic processes, consistent with recent studies indicating an overestimation of daily temperature extremes due to amplified diabatic heating from sensible heat fluxes (Röthlisberger et al., 2025). Also, Simpson et al. (2022) they argue that, in such regions, this is partly due to the limited representation of snow density, which affects the thermal conductance of the snow layer. In contrast, the underestimation in the tropics is primarily associated with biases in the adiabatic contribution and, consequently, in vertical motion, likely stemming from inadequate representation of convective processes and turbulent fluxes in the models (Bao & Stevens, 2021; Bergman & Sardeshmukh, 2004; Stohl, 1998). Similarly, during JJA, the widespread underestimation across most regions results mainly from a combination of underestimated advective and adiabatic processes. These seasonal and regional biases have important implications for targeted model development and improvement. Nevertheless, the general agreement between the spatial patterns of temperature variability in the CESM-LE and ERA5 increases confidence in future projections.

The projected DTDT variations and extremes reveal distinct seasonal and spatial differences. During DJF, projected DTDT changes follow a dipole pattern, characterised by weakening in mid- to high latitudes and intensification in the tropics. Also, during JJA, most tropical regions exhibit a significant intensification, but the signal in the extratropics is less coherent, with only a few regions, such as Greenland, western North America, eastern North America, and southern South America, experiencing a weakening in the magnitude of DTDT change. These results are similar to those of other recent studies on DTDT variations and extremes (Liu et al., 2025; Wang et al., 2025; Xu et al., 2020; Zhou et al., 2020). Furthermore, these projected changes in temperature variability in CESM-LE are generally similar to those in other CMIP5 and CMIP6 models (Bathiany et al., 2018; Tamarin-Brodsky et al., 2020; Wang et al., 2025; Xu et al., 2020). We further show how the changes in DTDT variations (σ_{DTDT}) can be decomposed into contributions from changes in the standard deviation of daily mean temperature (σ_T) and its autocorrelation ($r_{1,T}$). In particular, the projected σ_{DTDT} changes are mainly determined by σ_T changes during DJF and, in most regions, also during JJA. However, in some regions, changes in temporal autocorrelation also affect the magnitude of projected σ_{DTDT} change. For example, the projected large increase σ_{DTDT} over the tropics in DJF is due to a reduction in $r_{1,T}$. Conversely, a decrease in magnitude σ_{DTDT} over northern mid-latitude locations in JJA is associated with an increase in $r_{1,T}$. A similar future increase in autocorrelation over longer time scales is projected across these regions by other models (Li & Thompson, 2021), which may be linked to slow-moving weather patterns and the Arctic amplification (Kornhuber & Tamarin-Brodsky, 2021). These results indicate the need to further study projected changes in daily persistence using a multi-model ensemble.

Deleted: -

Moved (insertion) [1]

Deleted: ...Fig.... 1). The differences in daily standard deviations align with patterns observed in other models from the CMIP5 and CMIP6 initiatives (Bathiany et al., 2018; Giorgi & Raffaele, 2022). (... [69])

Formatted

Formatted: Font: Font color: Auto

Formatted: Font: Font color: Auto

Formatted: Font: Font color: Auto

Moved up [1]: The differences in daily standard deviations align with patterns observed in other models from the CMIP5 and CMIP6 initiatives (Bathiany et al., 2018; Giorgi & Raffaele, 2022).

Deleted: ... (Bathiany et al., 2018

Deleted: Simpson et al. (2022) argue that, in some regions, they are partly due to the limited representation of snow density, which affects the thermal conductance of the snow layer.

Deleted: -

Formatted: Font: Font color: Text 2

Deleted: projected future...rojected DTDT variations and extremes reveal distinct seasonal and spatial differences. During DJF, projected DTDT changes follow a dipole pattern, characterised by weakening in mid- (... [72])

Deleted: ...e However, we

Deleted:

Deleted: driven

Deleted: Furthermore, the projected σ_T changes in CESM-LE are generally similar to those in other CMIP5 models (Bathiany et al., 2018; Tamarin-Brodsky et al., 2020). H

Deleted: o...ever, in some regions, changes in temporal autocorrelation also affect ...ffect the magnitude of the (... [74])

Deleted: , even when the σ_T change is small

Deleted: in

Deleted: western Africa

Deleted: , whereas ... decrease in magnitude (... [75])

Deleted: Greenland and northwestern North America ...n JJA is linked...associated to...ith an increase of (... [76])

Deleted: ...A similar future increase in autocorrelation over longer time scales is projected across these regions western North America ...y other models (Li & Thompson, 2021), which may be linked to slow- (... [77])

Deleted: projected future...rojected changes in daily persistence further ...sing a multi- (... [78])

615 Additionally, we have examined in detail the physical mechanisms driving regional extreme DTD T changes during DJF and JJA using a combination of Eulerian composites and a Lagrangian temperature decomposition into contributions from advection, adiabatic and diabatic temperature changes. This detailed process analysis goes substantially beyond prior studies on extreme DTD T variations (Liu et al., 2025; Zhou et al., 2020). The physical processes observed in CESM-LE for historical simulations are generally similar to those in ERA5 (see also Part I), though with some differences in magnitude. The future weakening of both types of extremes (DTD T warming and cooling) over the extratropics during DJF is mainly due to a reduced contribution of advection, consistent with previous studies on general aspects of temperature variability (Tamarin-Brodsky et al., 2020; Wang et al., 2019; Wang et al., 2025). These changes are driven by a combination of subtle shifts in circulation patterns and changes in temperature gradients associated with Arctic amplification and changes in land-sea contrast (Figs. S7-11), leading to a decrease in DTD T variance (Chen et al., 2019; Dai & Deng, 2021; Garfinkel & Harnik, 2017; Screen, 2014; Zhou et al., 2020). For example, during future DTD T warming events over North America, synoptic flow anomalies weakened and propagated faster than during the historical period, with stronger southwesterly flow on day $t-1$ than on day t . Additionally, the projected temperature increase is greater over the more poleward air mass origins on day $t-1$ than on day t , most likely due to Arctic amplification (Fig. S6), which is more evident at high latitudes (Figs. S9 and 11). Both these factors reduce the DTD T variance. While advective changes predominate for these DTD T extremes, a minor contribution also arises from modifications in diabatic and adiabatic processes. Changes in diabatic processes, especially significant at the surface, are likely driven by variations in surface albedo and heat fluxes (Chen et al., 2019; Diro & Sushama, 2020).

630 The weakening of extreme DTD T changes during JJA shows clear regional and event-type differences, unlike the more uniform pattern in DJF. This trend is driven not only by changes in advection but also by significant contributions from both adiabatic and diabatic processes. During warming events, eastern North America experiences combined reductions in advection and diabatic heating, while western North America is mainly affected by a decrease in adiabatic warming. Similarly, cooling events show decreases in advection, along with region-specific changes: increased diabatic heating in the east and adiabatic warming in the west. Generally, in the Northern Hemisphere, the advection-driven changes (also see Fig. S15) associated with JJA extremes are likely linked to Arctic warming (Coumou et al., 2018; Kornhuber & Tamarin-Brodsky, 2021). The changes in diabatic processes are probably associated with changes in surface net radiative forcing, as discussed by Wang et al. (2025). Notably, despite the decline in extreme DTD T changes, daily heat extremes and heatwaves are still expected to intensify in the future (Bartusek et al., 2022; Heeter et al., 2023; White et al., 2023; Zhang et al., 2023). Overall, the reduction in extreme DTD T variability across extratropical regions in JJA results from a complex interaction of dynamical and thermodynamic factors, with their relative importance varying across regions and event types.

640 Conversely, an intensification of extreme DTD T variations is also evident in certain extratropical regions, particularly Northern Europe, Northern Asia, the south of Southern Africa and southern Australia (Figs. S22-24), where recent research indicates generally rising risks associated with temperature extremes (Beobide-Arsuaga et al., 2025; Chapman et al., 2024; Ciavarella

Deleted: The physical processes observed in CESM-LE for historical simulations are generally similar to those in ERA5 (see also Part I), thereby increasing confidence in future projections.

Deleted: -

Deleted: ,

Deleted: the

Deleted: compared

Deleted: to

Deleted: -

Deleted: In addition, the projected temperature increase is larger at the still more poleward air mass origins on day $t-1$ than on day t , most likely associated with Arctic amplification.

Formatted: Font: Italic

Formatted: Font: Italic

Deleted:

Deleted: -

Deleted: -

Deleted:

Deleted: -

Deleted: warming during summer as well

Deleted: , likely driven by intensified large-scale diabatic heating

Deleted: hose

Deleted: ies

Deleted: hemispheres,

Deleted: ,

Deleted: ern

Deleted:

Deleted: and

Deleted: 15-

Deleted: 16

et al., 2021; Nangombe et al., 2019). In the southern hemisphere, increased DTD extremes result from advection alone or in combination with adiabatic and diabatic processes, whereas changes in the northern high latitudes are primarily diabatic, with advection changes playing a role (mainly during warming events), while vertical motion remains largely unaffected. Also, the projected intensification at lower latitudes primarily results from enhanced diabatic processes, with advection playing a secondary role (Figs. S20–21). One important mechanism by which diabatic processes can influence temperature variability is through land-atmosphere interactions (Beobide-Arsuaga et al., 2025; Sato & Nakamura, 2019), leading to amplified temperature fluctuations and more frequent extremes, including extreme DTD changes (Cattiaux et al., 2015; Liu et al., 2025). For example, the future amplification of DTD warming events in central Europe is driven by increased diabatic heating on the event day, which closely resembles the mechanisms underlying the intensification of heatwaves (Schielicke & Pfahl, 2022). Heatwaves often occur in parallel with soil moisture depletion, which lowers the latent heat flux and increases the sensible heat flux through a higher Bowen ratio (Lin et al., 2022; Zscheischler & Seneviratne, 2017). Overall, these insights imply that regions such as the Sahel and central Europe could experience more pronounced soil drying in a warming climate (Elkouk et al., 2021; Ruosteenoja et al., 2018), possibly creating a feedback loop that amplifies future temperature extremes.

Similarly, an intensification in extreme DTD changes is projected in the tropics during DJF, highlighting increased risks for many developing countries. These regions are expected to encounter a disproportionate share of climate change's socioeconomic, agricultural, and health impacts (Bathiany et al., 2018; Ebi et al., 2025; Linsenmeier, 2023; Raymond et al., 2020). Historical and future extreme DTD changes over these areas are not driven by large-scale advection, but by local diabatic and adiabatic processes. The intensification of future DTD warming events is mainly caused by stronger local diabatic heating, linked to reduced cloud cover and precipitation on event days, which allows more solar radiation to reach the surface and raise temperatures—similar to processes during heatwaves (Birch et al., 2022; McKinnon et al., 2024; Moustakis et al., 2020). For future DTD cooling, local diabatic cooling remains relevant, whereas reduced adiabatic warming intensifies it. Nevertheless, such adiabatic changes and their influence on near-surface temperature might be linked to cloud-diabatic effects through lower-tropospheric static stability (Luo et al., 2024). Note, however, that these results have to be interpreted with care, since the trajectory calculations rely on resolved wind fields and therefore cannot capture the full spectrum of convective and turbulent motions. This limitation is especially pronounced in the tropics, where intense moist convection introduces significant uncertainty into the calculated transport pathways (Bao & Stevens, 2021; Bergman & Sardeshmukh, 2004; Stohl, 1998).

Our study is the first to apply a Lagrangian backwards-trajectory method to investigate the physical processes underlying projected extreme DTD changes. The results reveal clear seasonal and regional variations in the occurrence of these extremes, for which not only advection but also changes in adiabatic and diabatic processes are important. In the extratropics during DJF, reductions in extreme DTD changes are mainly attributable to weaker temperature advection, primarily linked to Arctic amplification. Conversely, the weakening of extremes during JJA is caused not only by advection but also by diabatic and

Deleted: the combined influences of

Deleted: ,

Deleted: ,

Deleted: some

Deleted: 13-

Deleted: 14

Deleted: -

Deleted:

Deleted: -

Deleted: -

Deleted: -

Deleted: -

Deleted: 1

Deleted: -

Deleted: projected future

Deleted: Conversely, the weakening of extremes during JJA is primarily driven by diabatic and adiabatic processes

adiabatic processes. In contrast, there is substantial intensification of DTD extremes over tropical and subtropical land areas during JJA, mainly driven by diabatic processes that are likely associated with changes in surface fluxes. Adiabatic warming changes, combined with diabatic processes, are crucial for the increase in tropical extremes during DJF. These findings highlight the importance of accounting for the Lagrangian temperature change of air masses when examining spatial and seasonal variations in future DTD changes, which can significantly affect ecosystems, public health, and infrastructure. They also emphasise the need for region-specific adaptation strategies to mitigate the risks associated with rapid temperature changes.

Deleted: , with some changes in advection, especially in North America

Deleted: of extremes

Deleted: he

Deleted: tropic

Deleted: -

Code and data availability

The code for the trajectory model LAGRANTO is available at <https://iacweb.ethz.ch/staff/sprenger/lagranto/> (Sprenger & Wernli, 2015). The model code for CESM version 1 used for the ensemble simulation is available from (Kay et al., 2015); <https://www2.cesm.ucar.edu/models/cesm1.0/>. ERA5 data are available via the Copernicus Climate Change Service (Hersbach et al., 2020); <https://doi.org/10.24381/cds.143582cf>.

Author contributions

Both authors designed the study. KH performed the analysis, produced the figures, and drafted the manuscript. Both authors discussed the results and edited the manuscript.

Competing interests

Stephan Pfahl is executive editor of WCD.

Acknowledgments

We acknowledge the HPC service of ZEDAT, Freie Universität Berlin, for providing computational Resources (Bennett et al., 2020). [We are grateful to two anonymous reviewers whose constructive comments helped us to improve the paper.](#)

References

Bao, J., & Stevens, B. (2021). The Elements of the Thermodynamic Structure of the Tropical Atmosphere. *Journal of the Meteorological Society of Japan. Ser. II*, 99(6), 1483-1499. <https://doi.org/10.2151/jmsj.2021-072>

- 1755 Bartusek, S., Kornhuber, K., & Ting, M. (2022). 2021 North American heatwave amplified by climate change-driven nonlinear interactions. *Nature Climate Change*, 12(12), 1143-1150. <https://doi.org/10.1038/s41558-022-01520-4>
- Bathiany, S., Dakos, V., Scheffer, M., & Lenton, T. M. (2018). Climate models predict increasing temperature variability in poor countries. *Science Advances*, 4(5), eaar5809. <https://doi.org/doi:10.1126/sciadv.aar5809>
- Bennett, L., Melchers, B., & Proppe, B. (2020). Curta: a general-purpose high-performance computer at ZEDAT, Freie Universität Berlin.
- 1760 Beobide-Arsuaga, G., Suarez-Gutierrez, L., Barkhordarian, A., Olonscheck, D., & Baehr, J. (2025). Increasing central and northern European summer heatwave intensity due to forced changes in internal variability. *Nature Communications*, 16(1), 9485. <https://doi.org/10.1038/s41467-025-65392-w>
- Bergman, J. W., & Sardeshmukh, P. D. (2004). Dynamic Stabilization of Atmospheric Single Column Models. *Journal of Climate*, 17(5), 1004-1021. [https://doi.org/https://doi.org/10.1175/1520-0442\(2004\)017<1004:DSOASC>2.0.CO;2](https://doi.org/https://doi.org/10.1175/1520-0442(2004)017<1004:DSOASC>2.0.CO;2)
- 1765 Bieli, M., Pfahl, S., & Wernli, H. (2015). A Lagrangian investigation of hot and cold temperature extremes in Europe. *Quarterly Journal of the Royal Meteorological Society*, 141(686), 98-108. <https://doi.org/https://doi.org/10.1002/qj.2339>
- 1770 Birch, C. E., Jackson, L. S., Finney, D. L., Marsham, J. M., Stratton, R. A., Tucker, S., Chapman, S., Senior, C. A., Keane, R. J., Guichard, F., & Kendon, E. J. (2022). Future Changes in African Heatwaves and Their Drivers at the Convective Scale. *Journal of Climate*, 35(18), 5981-6006. <https://doi.org/https://doi.org/10.1175/JCLI-D-21-0790.1>
- Brunner, L., Schaller, N., Anstey, J., Sillmann, J., & Steiner, A. K. (2018). Dependence of Present and Future European Temperature Extremes on the Location of Atmospheric Blocking. *Geophysical Research Letters*, 45(12), 6311-6320. <https://doi.org/https://doi.org/10.1029/2018GL077837>
- 1775 Cattiaux, J., Douville, H., Schoetter, R., Parey, S., & Yiou, P. (2015). Projected increase in diurnal and interdiurnal variations of European summer temperatures. *Geophysical Research Letters*, 42(3), 899-907. <https://doi.org/https://doi.org/10.1002/2014GL062531>
- Chan, E. Y. Y., Goggins, W. B., Kim, J. J., & Griffiths, S. M. (2012). A study of intracity variation of temperature-related mortality and socioeconomic status among the Chinese population in Hong Kong. *Journal of Epidemiology and Community Health*, 66(4), 322-327. <https://doi.org/10.1136/jech.2008.085167>
- 1780 Chan, P. W., Catto, J. L., & Collins, M. (2022). Heatwave–blocking relation change likely dominates over decrease in blocking frequency under global warming. *npj Climate and Atmospheric Science*, 5(1), 68. <https://doi.org/10.1038/s41612-022-00290-2>
- 1785 Chapman, S., Syktus, J., Trancoso, R., Toombs, N., & Eccles, R. (2024). Projected changes in mean climate and extremes from downscaled high-resolution CMIP6 simulations in Australia. *Weather and Climate Extremes*, 46, 100733. <https://doi.org/https://doi.org/10.1016/j.wace.2024.100733>

- Chen, H., Yang, J., Tan, C., Wang, J., & Cai, X. (2025). Dynamic evolution of Day-To-Day Temperature fluctuations and population exposure on a global scale. *PLoS One*, 20(11), e0333887. <https://doi.org/10.1371/journal.pone.0333887>
- 1790 Chen, J., Dai, A., & Zhang, Y. (2019). Projected Changes in Daily Variability and Seasonal Cycle of Near-Surface Air Temperature over the Globe during the Twenty-First Century. *Journal of Climate*, 32(24), 8537-8561. <https://doi.org/https://doi.org/10.1175/JCLI-D-19-0438.1>
- Ciavarella, A., Cotterill, D., Stott, P., Kew, S., Philip, S., van Oldenborgh, G. J., Skålevåg, A., Lorenz, P., Robin, Y., Otto, F., Hauser, M., Seneviratne, S. I., Lehner, F., & Zolina, O. (2021). Prolonged Siberian heat of 2020 almost impossible without human influence. *Climatic Change*, 166(1), 9. <https://doi.org/10.1007/s10584-021-03052-w>
- 1795 Coumou, D., Di Capua, G., Vavrus, S., Wang, L., & Wang, S. (2018). The influence of Arctic amplification on mid-latitude summer circulation. *Nature Communications*, 9(1), 2959. <https://doi.org/10.1038/s41467-018-05256-8>
- Dai, A., & Deng, J. (2021). Arctic Amplification Weakens the Variability of Daily Temperatures over Northern Middle-High Latitudes. *Journal of Climate*, 34(7), 2591-2609. <https://doi.org/https://doi.org/10.1175/JCLI-D-20-0514.1>
- Diro, G. T., & Sushama, L. (2020). Contribution of Snow Cover Decline to Projected Warming Over North America. *Geophysical Research Letters*, 47(1), e2019GL084414. <https://doi.org/https://doi.org/10.1029/2019GL084414>
- 1800 Dolores-Tesillos, E., Teubler, F., & Pfahl, S. (2022). Future changes in North Atlantic winter cyclones in CESM-LE – Part 1: Cyclone intensity, potential vorticity anomalies, and horizontal wind speed. *Weather Clim. Dynam.*, 3(2), 429-448. <https://doi.org/10.5194/wcd-3-429-2022>
- 1805 Ebi, K., Haines, A., Andrade, R. F. S., Åström, C., Barreto, M. L., Bonell, A., Brink, N., Caminade, C., Carlson, C. J., Carter, R., Chua, P., Cissé, G., Colón-González, F. J., Dasgupta, S., Galvao, L. A., Garrido Zornoza, M., Gasparrini, A., Gordon-Strachan, G., Hajat, S.,...Stuart-Smith, R. F. (2025). The attribution of human health outcomes to climate change: a transdisciplinary guidance document. *Clim Change*, 178(8). <https://doi.org/10.1007/s10584-025-03976-7>
- Elkouk, A., El Morjani, Z. E. A., Pokhrel, Y., Chehbouni, A., Sifeddine, A., Thober, S., & Bouchaou, L. (2021). Multi-model ensemble projections of soil moisture drought over North Africa and the Sahel region under 1.5, 2, and 3 °C global warming. *Climatic Change*, 167(3), 52. <https://doi.org/10.1007/s10584-021-03202-0>
- 1810 Garfinkel, C. I., & Harnik, N. (2017). The Non-Gaussianity and Spatial Asymmetry of Temperature Extremes Relative to the Storm Track: The Role of Horizontal Advection. *Journal of Climate*, 30(2), 445-464. <https://doi.org/https://doi.org/10.1175/JCLI-D-15-0806.1>
- 1815 Giorgi, F., & Raffaele, F. (2022). On the dependency of GCM-based regional surface climate change projections on model biases, resolution and climate sensitivity. *Climate Dynamics*, 58(9), 2843-2862. <https://doi.org/10.1007/s00382-021-06037-8>
- Hamal, K., & Pfahl, S. (2025). Physical processes leading to extreme day-to-day temperature change – Part 1: Present-day climate. *Weather Clim. Dynam.*, 6(3), 879-899. <https://doi.org/10.5194/wcd-6-879-2025>

- 1820 Hartig, K., Tziperman, E., & Loughner, C. P. (2023). Processes Contributing to North American Cold Air Outbreaks Based on Air Parcel Trajectory Analysis. *Journal of Climate*, 36(3), 931-943. <https://doi.org/https://doi.org/10.1175/JCLI-D-22-0204.1>
- Heeter, K. J., Harley, G. L., Abatzoglou, J. T., Anchukaitis, K. J., Cook, E. R., Coulthard, B. L., Dye, L. A., & Homfeld, I. K. (2023). Unprecedented 21st century heat across the Pacific Northwest of North America. *npj Climate and Atmospheric Science*, 6(1), 5. <https://doi.org/10.1038/s41612-023-00340-3>
- 1825 Hersbach, H., Bell, B., Berrisford, P., Hirahara, S., Horányi, A., Muñoz-Sabater, J., Nicolas, J., Peubey, C., Radu, R., Schepers, D., Simmons, A., Soci, C., Abdalla, S., Abellan, X., Balsamo, G., Bechtold, P., Biavati, G., Bidlot, J., Bonavita, M.,...Thépaut, J.-N. (2020). The ERA5 global reanalysis. *Quarterly Journal of the Royal Meteorological Society*, 146(730), 1999-2049. <https://doi.org/https://doi.org/10.1002/qj.3803>
- Hovdahl, I. (2022). The deadly effect of day-to-day temperature variation in the United States. *Environmental Research Letters*, 17(10), 104031. <https://doi.org/10.1088/1748-9326/ac9297>
- 1830 Intergovernmental Panel on Climate, C. (2023). *Climate Change 2022 – Impacts, Adaptation and Vulnerability: Working Group II Contribution to the Sixth Assessment Report of the Intergovernmental Panel on Climate Change*. Cambridge University Press. <https://doi.org/DOI:10.1017/9781009325844>
- Jeong, D. I., Yu, B., & Cannon, A. J. (2025). Future Changes in North American Summer Heatwave Variability and Associated Dynamic and Thermodynamic Processes. *Journal of Climate*, 38(22), 6727-6744. <https://doi.org/https://doi.org/10.1175/JCLI-D-25-0114.1>
- 1835 Kautz, L. A., Martius, O., Pfahl, S., Pinto, J. G., Ramos, A. M., Sousa, P. M., & Woollings, T. (2022). Atmospheric blocking and weather extremes over the Euro-Atlantic sector – a review. *Weather Clim. Dynam.*, 3(1), 305-336. <https://doi.org/10.5194/wcd-3-305-2022>
- 1840 Kay, J. E., Deser, C., Phillips, A., Mai, A., Hannay, C., Strand, G., Arblaster, J. M., Bates, S. C., Danabasoglu, G., Edwards, J., Holland, M., Kushner, P., Lamarque, J.-F., Lawrence, D., Lindsay, K., Middleton, A., Muñoz, E., Neale, R., Oleson, K.,...Vertenstein, M. (2015). The Community Earth System Model (CESM) Large Ensemble Project: A Community Resource for Studying Climate Change in the Presence of Internal Climate Variability. *Bulletin of the American Meteorological Society*, 96(8), 1333-1349. <https://doi.org/https://doi.org/10.1175/BAMS-D-13-00255.1>
- 1845 Kim, O.-Y., Wang, B., & Shin, S.-H. (2013). How do weather characteristics change in a warming climate? *Climate Dynamics*, 41(11), 3261-3281. <https://doi.org/10.1007/s00382-013-1795-8>
- Kornhuber, K., & Tamarin-Brodsky, T. (2021). Future Changes in Northern Hemisphere Summer Weather Persistence Linked to Projected Arctic Warming. *Geophysical Research Letters*, 48(4), e2020GL091603. <https://doi.org/https://doi.org/10.1029/2020GL091603>
- 1850 Kotz, M., Wenz, L., Stechemesser, A., Kalkuhl, M., & Levermann, A. (2021). Day-to-day temperature variability reduces economic growth. *Nature Climate Change*, 11(4), 319-325. <https://doi.org/10.1038/s41558-020-00985-5>

- Lin, H., Li, Y., & Zhao, L. (2022). Partitioning of Sensible and Latent Heat Fluxes in Different Vegetation Types and Their Spatiotemporal Variations Based on 203 FLUXNET Sites. *Journal of Geophysical Research: Atmospheres*, 127(21), e2022JD037142. <https://doi.org/https://doi.org/10.1029/2022JD037142>
- 1855 Linsenmeier, M. (2023). Temperature variability and long-run economic development. *Journal of Environmental Economics and Management*, 121, 102840. <https://doi.org/https://doi.org/10.1016/j.jeem.2023.102840>
- | <https://doi.org/https://doi.org/10.1038/s41558-025-02486-9> Liu, Q., Fu, C., Xu, Z., & Ding, A. (2025). Global warming intensifies extreme day-to-day temperature changes in mid-low latitudes. *Nature Climate Change*. <https://doi.org/10.1038/s41558-025-02486-9>
- Luo, H., Quaas, J., & Han, Y. (2024). Diurnally asymmetric cloud cover trends amplify greenhouse warming. *Science Advances*, 10(25), eado5179. <https://doi.org/doi:10.1126/sciadv.ado5179>
- 1860 Martínez-Solanas, È., Quijal-Zamorano, M., Achebak, H., Petrova, D., Robine, J.-M., Herrmann, F. R., Rodó, X., & Ballester, J. (2021). Projections of temperature-attributable mortality in Europe: a time series analysis of 147 contiguous regions in 16 countries. *The Lancet Planetary Health*, 5(7), e446-e454. [https://doi.org/10.1016/S2542-5196\(21\)00150-9](https://doi.org/10.1016/S2542-5196(21)00150-9)
- Mayer, A. (2025). A New Global Lagrangian Analysis of Near-Surface Temperature Extremes. *Geophysical Research Letters*, 52(19), e2025GL116696. <https://doi.org/https://doi.org/10.1029/2025GL116696>
- 1865 McKinnon, K. A., Simpson, I. R., & Williams, A. P. (2024). The pace of change of summertime temperature extremes. *Proceedings of the National Academy of Sciences*, 121(42), e2406143121. <https://doi.org/doi:10.1073/pnas.2406143121>
- 1870 Moustakis, Y., Onof, C. J., & Paschalis, A. (2020). Atmospheric convection, dynamics and topography shape the scaling pattern of hourly rainfall extremes with temperature globally. *Communications Earth & Environment*, 1(1), 11. <https://doi.org/10.1038/s43247-020-0003-0>
- Nangombe, S. S., Zhou, T., Zhang, W., Zou, L., & Li, D. (2019). High-Temperature Extreme Events Over Africa Under 1.5 and 2 °C of Global Warming. *Journal of Geophysical Research: Atmospheres*, 124(8), 4413-4428. <https://doi.org/https://doi.org/10.1029/2018JD029747>
- 1875 Neal, E., Huang, C. S. Y., & Nakamura, N. (2022). The 2021 Pacific Northwest Heat Wave and Associated Blocking: Meteorology and the Role of an Upstream Cyclone as a Diabatic Source of Wave Activity. *Geophysical Research Letters*, 49(8), e2021GL097699. <https://doi.org/https://doi.org/10.1029/2021GL097699>
- Nygård, T., Papritz, L., Naakka, T., & Vihma, T. (2023). Cold wintertime air masses over Europe: where do they come from and how do they form? *Weather Clim. Dynam.*, 4(4), 943-961. <https://doi.org/10.5194/wcd-4-943-2023>
- 1880 Papritz, L., & Spengler, T. (2017). A Lagrangian Climatology of Wintertime Cold Air Outbreaks in the Irminger and Nordic Seas and Their Role in Shaping Air-Sea Heat Fluxes. *Journal of Climate*, 30(8), 2717-2737. <https://doi.org/https://doi.org/10.1175/JCLI-D-16-0605.1>

Formatted: German

- Quinting, J. F., & Reeder, M. J. (2017). Southeastern Australian Heat Waves from a Trajectory Viewpoint. *Monthly Weather Review*, 145(10), 4109-4125. <https://doi.org/https://doi.org/10.1175/MWR-D-17-0165.1>
- 1885 Raymond, C., Matthews, T., & Horton, R. M. (2020). The emergence of heat and humidity too severe for human tolerance. *Sci Adv*, 6(19), eaaw1838. <https://doi.org/10.1126/sciadv.aaw1838>
- Röthlisberger, M., & Papritz, L. (2023a). A Global Quantification of the Physical Processes Leading to Near-Surface Cold Extremes. *Geophysical Research Letters*, 50(5), e2022GL101670. <https://doi.org/https://doi.org/10.1029/2022GL101670>
- 1890 Röthlisberger, M., & Papritz, L. (2023b). Quantifying the physical processes leading to atmospheric hot extremes at a global scale. *Nature Geoscience*, 16(3), 210-216. <https://doi.org/10.1038/s41561-023-01126-1>
- Röthlisberger, M., Sprenger, M., Beyerle, U., Fischer, E. M., & Wernli, H. (2025). Advective, adiabatic and diabatic contributions to heat extremes simulated with the Community Earth System Model version 2. *EGU Sphere*, 2025, 1-32. <https://doi.org/10.5194/egusphere-2025-5146>
- 1895 Ruosteenoja, K., Markkanen, T., Venäläinen, A., Räisänen, P., & Peltola, H. (2018). Seasonal soil moisture and drought occurrence in Europe in CMIP5 projections for the 21st century. *Climate Dynamics*, 50(3), 1177-1192. <https://doi.org/10.1007/s00382-017-3671-4>
- Sato, T., & Nakamura, T. (2019). Intensification of hot Eurasian summers by climate change and land-atmosphere interactions. *Scientific Reports*, 9(1), 10866. <https://doi.org/10.1038/s41598-019-47291-5>
- 1900 Schaller, N., Sillmann, J., Anstey, J., Fischer, E. M., Grams, C. M., & Russo, S. (2018). Influence of blocking on Northern European and Western Russian heatwaves in large climate model ensembles. *Environmental Research Letters*, 13(5), 054015. <https://doi.org/10.1088/1748-9326/aaba55>
- Schielicke, L., & Pfahl, S. (2022). European heatwaves in present and future climate simulations: a Lagrangian analysis. *Weather Clim. Dynam.*, 3(4), 1439-1459. <https://doi.org/10.5194/wcd-3-1439-2022>
- 1905 Screen, J. A. (2014). Arctic amplification decreases temperature variance in northern mid- to high-latitudes. *Nature Climate Change*, 4(7), 577-582. <https://doi.org/10.1038/nclimate2268>
- Simpson, I. R., Lawrence, D. M., Swenson, S. C., Hannay, C., McKinnon, K. A., & Truesdale, J. E. (2022). Improvements in Wintertime Surface Temperature Variability in the Community Earth System Model Version 2 (CESM2) Related to the Representation of Snow Density. *Journal of Advances in Modeling Earth Systems*, 14(4), e2021MS002880. <https://doi.org/https://doi.org/10.1029/2021MS002880>
- 1910 Sprenger, M., & Wernli, H. (2015). The LAGRANTO Lagrangian analysis tool – version 2.0. *Geosci. Model Dev.*, 8(8), 2569-2586. <https://doi.org/10.5194/gmd-8-2569-2015>
- Stohl, A. (1998). Computation, accuracy and applications of trajectories—A review and bibliography. *Atmospheric Environment*, 32(6), 947-966. [https://doi.org/https://doi.org/10.1016/S1352-2310\(97\)00457-3](https://doi.org/https://doi.org/10.1016/S1352-2310(97)00457-3)

- 1915 Tamarin-Brodsky, T., Hodges, K., Hoskins, B. J., & Shepherd, T. G. (2020). Changes in Northern Hemisphere temperature variability shaped by regional warming patterns. *Nature Geoscience*, 13(6), 414–421. <https://doi.org/10.1038/s41561-020-0576-3>
- Vogel, M. M., Zscheischler, J., Fischer, E. M., & Seneviratne, S. I. (2020). Development of Future Heatwaves for Different Hazard Thresholds. *Journal of Geophysical Research: Atmospheres*, 125(9), e2019JD032070. <https://doi.org/https://doi.org/10.1029/2019JD032070>
- 1920 Wan, H., Kirchmeier-Young, M. C., & Zhang, X. (2021). Human influence on daily temperature variability over land. *Environmental Research Letters*, 16(9), 094026. <https://doi.org/10.1088/1748-9326/ac1cb9>
- Wang, F., Vavrus, S. J., Francis, J. A., & Martin, J. E. (2019). The role of horizontal thermal advection in regulating wintertime mean and extreme temperatures over interior North America during the past and future. *Climate Dynamics*, 53(9), 6125–6144. <https://doi.org/10.1007/s00382-019-04917-8>
- 1925 Wang, J., Zhang, J., & Zhang, P. (2022). Rising temperature threatens China’s cropland. *Environmental Research Letters*, 17(8), 084042. <https://doi.org/10.1088/1748-9326/ac84f1>
- Wang, P., Ye, F., Yang, Y., Tang, J., & Liao, H. (2025). Mitigated Rapid Temperature Variability in the Northern Mid-High Latitudes Under Carbon Neutrality. *Geophysical Research Letters*, 52(20), e2025GL118040. <https://doi.org/https://doi.org/10.1029/2025GL118040>
- 1930 White, R. H., Anderson, S., Booth, J. F., Braich, G., Draeger, C., Fei, C., Harley, C. D. G., Henderson, S. B., Jakob, M., Lau, C.-A., Mareshet Admasu, L., Narinesingh, V., Rodell, C., Roocroft, E., Weinberger, K. R., & West, G. (2023). The unprecedented Pacific Northwest heatwave of June 2021. *Nature Communications*, 14(1), 727. <https://doi.org/10.1038/s41467-023-36289-3>
- 1935 Wilks, D. S. (2016). “The Stippling Shows Statistically Significant Grid Points”: How Research Results are Routinely Overstated and Overinterpreted, and What to Do about It. *Bulletin of the American Meteorological Society*, 97(12), 2263–2273. <https://doi.org/https://doi.org/10.1175/BAMS-D-15-00267.1>
- 1940 Wu, Y., Wen, B., Li, S., Gasparrini, A., Tong, S., Overcenco, A., Urban, A., Schneider, A., Entezari, A., Vicedo-Cabrera, A. M., Zanobetti, A., Analitis, A., Zeka, A., Tobias, A., Alahmad, B., Armstrong, B., Forsberg, B., Iñiguez, C., Ameling, C.,...Guo, Y. (2022). Fluctuating temperature modifies heat-mortality association around the globe. *The Innovation*, 3(2), 100225. <https://doi.org/https://doi.org/10.1016/j.xinn.2022.100225>
- Xu, Z., Huang, F., Liu, Q., & Fu, C. (2020). Global pattern of historical and future changes in rapid temperature variability. *Environmental Research Letters*, 15(12), 124073. <https://doi.org/10.1088/1748-9326/abccf3>
- Zhang, X., Zhou, T., Zhang, W., Ren, L., Jiang, J., Hu, S., Zuo, M., Zhang, L., & Man, W. (2023). Increased impact of heat domes on 2021-like heat extremes in North America under global warming. *Nature Communications*, 14(1), 1690. <https://doi.org/10.1038/s41467-023-37309-y>

Zhou, X., Wang, Q., & Yang, T. (2020). Decreases in days with sudden day-to-day temperature change in the warming world. *Global and Planetary Change*, 192, 103239. <https://doi.org/https://doi.org/10.1016/j.gloplacha.2020.103239>

Zou, Z., Li, C., Wu, X., Meng, Z., & Cheng, C. (2024). The effect of day-to-day temperature variability on agricultural productivity. *Environmental Research Letters*, 19(12), 124046. <https://doi.org/10.1088/1748-9326/ad8ede>

1950 Zscheischler, J., & Seneviratne, S. I. (2017). Dependence of drivers affects risks associated with compound events. *Science Advances*, 3(6), e1700263. <https://doi.org/doi:10.1126/sciadv.1700263>

Zschenderlein, P., Fink, A. H., Pfahl, S., & Wernli, H. (2019). Processes determining heat waves across different European climates. *Quarterly Journal of the Royal Meteorological Society*, 145(724), 2973-2989. <https://doi.org/https://doi.org/10.1002/qj.3599>

1955

▼
▲
Page 6: [1] Deleted **Hamal** **3/23/26 5:29:00 PM**

▼
▲
Page 6: [1] Deleted **Hamal** **3/23/26 5:29:00 PM**

▼
▲
Page 6: [1] Deleted **Hamal** **3/23/26 5:29:00 PM**

▼
▲
Page 6: [1] Deleted **Hamal** **3/23/26 5:29:00 PM**

▼
▲
Page 6: [1] Deleted **Hamal** **3/23/26 5:29:00 PM**

▼
▲
Page 6: [1] Deleted **Hamal** **3/23/26 5:29:00 PM**

▼
▲
Page 6: [1] Deleted **Hamal** **3/23/26 5:29:00 PM**

▼
▲
Page 6: [1] Deleted **Hamal** **3/23/26 5:29:00 PM**

▼
▲
Page 6: [2] Formatted **Hamal** **3/5/26 2:45:00 PM**

Font: Font color: Auto, English (US)

▼
▲
Page 6: [2] Formatted **Hamal** **3/5/26 2:45:00 PM**

Font: Font color: Auto, English (US)

▼
▲
Page 6: [3] Deleted **Hamal** **3/5/26 2:44:00 PM**

▼
▲
Page 6: [3] Deleted **Hamal** **3/5/26 2:44:00 PM**

▼
▲
Page 6: [3] Deleted **Hamal** **3/5/26 2:44:00 PM**

▼
▲
Page 6: [3] Deleted **Hamal** **3/5/26 2:44:00 PM**

▼
▲
Page 6: [3] Deleted **Hamal** **3/5/26 2:44:00 PM**

▼
▲
Page 6: [3] Deleted **Hamal** **3/5/26 2:44:00 PM**

▼
▲
Page 6: [4] Formatted **Hamal** **3/19/26 6:44:00 AM**

Font: Font color: Auto, English (US)

▲
Page 6: [4] Formatted **Hamal** **3/19/26 6:44:00 AM**

Font: Font color: Auto, English (US)

▲
Page 6: [4] Formatted **Hamal** **3/19/26 6:44:00 AM**

Font: Font color: Auto, English (US)

▲
Page 6: [4] Formatted **Hamal** **3/19/26 6:44:00 AM**

Font: Font color: Auto, English (US)

▲
Page 6: [5] Deleted **Hamal** **3/5/26 2:37:00 PM**

▼
▲
Page 6: [5] Deleted **Hamal** **3/5/26 2:37:00 PM**

▼
▲
Page 6: [5] Deleted **Hamal** **3/5/26 2:37:00 PM**

▼
▲
Page 6: [5] Deleted **Hamal** **3/5/26 2:37:00 PM**

▼
▲
Page 6: [5] Deleted **Hamal** **3/5/26 2:37:00 PM**

▼
▲
Page 6: [5] Deleted **Hamal** **3/5/26 2:37:00 PM**

▼
▲
Page 6: [5] Deleted **Hamal** **3/5/26 2:37:00 PM**

▼
▲
Page 6: [5] Deleted **Hamal** **3/5/26 2:37:00 PM**

▼
▲
Page 6: [5] Deleted **Hamal** **3/5/26 2:37:00 PM**

▼
▲

Page 6: [6] Formatted **Hamal** **3/19/26 6:48:00 AM**

Font: 10 pt, English (US)

▲ **Page 6: [6] Formatted** **Hamal** **3/19/26 6:48:00 AM**

Font: 10 pt, English (US)

▲ **Page 6: [6] Formatted** **Hamal** **3/19/26 6:48:00 AM**

Font: 10 pt, English (US)

▲ **Page 6: [6] Formatted** **Hamal** **3/19/26 6:48:00 AM**

Font: 10 pt, English (US)

▲ **Page 7: [7] Deleted** **Hamal** **3/19/26 6:48:00 AM**

▼

▲

Page 7: [8] Deleted **Hamal** **3/19/26 6:55:00 AM**

▼

▲ **Page 7: [9] Formatted** **Hamal** **3/9/26 10:02:00 AM**

Font: (Default) Times New Roman, Font color: Auto, Pattern: Clear

▲ **Page 7: [10] Formatted** **Hamal** **3/9/26 10:02:00 AM**

Font: (Default) Times New Roman, Font color: Auto, Pattern: Clear

▲ **Page 8: [11] Formatted** **Hamal** **3/9/26 11:29:00 AM**

Font: (Default) Times New Roman, Font color: Auto

▲ **Page 8: [12] Formatted** **Hamal** **3/9/26 11:29:00 AM**

Font: (Default) Times New Roman, Font color: Auto

▲ **Page 8: [13] Formatted** **Hamal** **3/9/26 11:29:00 AM**

Font: (Default) Times New Roman, Font color: Auto

▲ **Page 8: [14] Formatted** **Hamal** **3/9/26 11:29:00 AM**

Font: (Default) Times New Roman, Font color: Auto

▲ **Page 8: [15] Formatted** **Hamal** **3/9/26 11:29:00 AM**

Font: (Default) Times New Roman, Font color: Auto

▲ **Page 9: [16] Deleted** **Hamal** **3/18/26 1:46:00 PM**

✖ **Page 9: [17] Deleted** **Hamal** **3/9/26 9:44:00 AM**

▼
Page 10: [18] Deleted **Hamal** **3/23/26 5:29:00 PM**

▲
Page 10: [18] Deleted **Hamal** **3/23/26 5:29:00 PM**

▼
▲
Page 10: [18] Deleted **Hamal** **3/23/26 5:29:00 PM**

▼
▲
Page 10: [18] Deleted **Hamal** **3/23/26 5:29:00 PM**

▼
▲
Page 10: [18] Deleted **Hamal** **3/23/26 5:29:00 PM**

▼
▲
Page 10: [18] Deleted **Hamal** **3/23/26 5:29:00 PM**

▼
▲
Page 10: [18] Deleted **Hamal** **3/23/26 5:29:00 PM**

▼
▲
Page 10: [19] Formatted **Hamal** **3/24/26 1:49:00 PM**

Font: 9 pt, Not Bold

▲
Page 10: [19] Formatted **Hamal** **3/24/26 1:49:00 PM**

Font: 9 pt, Not Bold

▲
Page 10: [19] Formatted **Hamal** **3/24/26 1:49:00 PM**

Font: 9 pt, Not Bold

▲
Page 10: [19] Formatted **Hamal** **3/24/26 1:49:00 PM**

Font: 9 pt, Not Bold

▲
Page 10: [19] Formatted **Hamal** **3/24/26 1:49:00 PM**

Font: 9 pt, Not Bold

▲
Page 10: [19] Formatted **Hamal** **3/24/26 1:49:00 PM**

Font: 9 pt, Not Bold

▲
Page 10: [19] Formatted **Hamal** **3/24/26 1:49:00 PM**

Font: 9 pt, Not Bold

▲
Page 10: [19] Formatted **Hamal** **3/24/26 1:49:00 PM**

Font: 9 pt, Not Bold

▲
Page 10: [19] Formatted **Hamal** **3/24/26 1:49:00 PM**

Font: 9 pt, Not Bold

▲
Page 10: [20] Deleted **Hamal** **3/20/26 12:53:00 PM**

✖
▲

Page 10: [20] Deleted **Hamal** **3/20/26 12:53:00 PM**

✖
▲

Page 10: [21] Deleted **Hamal** **3/20/26 12:54:00 PM**

✖
▲

Page 10: [21] Deleted **Hamal** **3/20/26 12:54:00 PM**

✖
▲

Page 11: [22] Deleted **Hamal** **3/23/26 8:36:00 AM**

✖
Page 11: [23] Deleted **Hamal** **3/23/26 9:53:00 AM**

✖
Page 12: [24] Deleted **Hamal** **3/9/26 12:57:00 PM**

▼

▲
Page 15: [25] Formatted **Hamal** **3/23/26 6:59:00 PM**

Font: Not Bold

▲
Page 15: [25] Formatted **Hamal** **3/23/26 6:59:00 PM**

Font: Not Bold

▲
Page 15: [25] Formatted **Hamal** **3/23/26 6:59:00 PM**

Font: Not Bold

▲
Page 15: [25] Formatted **Hamal** **3/23/26 6:59:00 PM**

Font: Not Bold

▲
Page 15: [25] Formatted **Hamal** **3/23/26 6:59:00 PM**

Font: Not Bold

▲
Page 15: [25] Formatted **Hamal** **3/23/26 6:59:00 PM**

Font: Not Bold

▲
Page 15: [25] Formatted **Hamal** **3/23/26 6:59:00 PM**

Font: Not Bold

▲
Page 15: [25] Formatted **Hamal** **3/23/26 6:59:00 PM**

Font: Not Bold

▲
Page 15: [25] Formatted **Hamal** **3/23/26 6:59:00 PM**

Font: Not Bold

▲
Page 15: [25] Formatted **Hamal** **3/23/26 6:59:00 PM**

Font: Not Bold

▲
Page 15: [25] Formatted **Hamal** **3/23/26 6:59:00 PM**

Font: Not Bold

▲
Page 15: [25] Formatted **Hamal** **3/23/26 6:59:00 PM**

Font: Not Bold

▲
Page 15: [26] Formatted **Hamal** **3/23/26 6:59:00 PM**

Font: Not Bold, English (UK)

▲
Page 15: [26] Formatted **Hamal** **3/23/26 6:59:00 PM**

Font: Not Bold, English (UK)

▲
Page 15: [27] Formatted **Hamal** **3/23/26 6:59:00 PM**

Font: Not Bold, English (UK)

▲
Page 15: [27] Formatted **Hamal** **3/23/26 6:59:00 PM**

Font: Not Bold, English (UK)

▲
Page 15: [28] Formatted **Hamal** **3/23/26 6:59:00 PM**

Font: Not Bold

▲
Page 15: [28] Formatted **Hamal** **3/23/26 6:59:00 PM**

Font: Not Bold

▲
Page 15: [28] Formatted **Hamal** **3/23/26 6:59:00 PM**

Font: Not Bold

▲
Page 15: [28] Formatted **Hamal** **3/23/26 6:59:00 PM**

Font: Not Bold

▲
Page 15: [28] Formatted **Hamal** **3/23/26 6:59:00 PM**

Font: Not Bold

▲

Page 15: [28] Formatted **Hamal** **3/23/26 6:59:00 PM**

Font: Not Bold

▲ **Page 15: [28] Formatted** **Hamal** **3/23/26 6:59:00 PM**

Font: Not Bold

▲ **Page 15: [28] Formatted** **Hamal** **3/23/26 6:59:00 PM**

Font: Not Bold

▲ **Page 15: [28] Formatted** **Hamal** **3/23/26 6:59:00 PM**

Font: Not Bold

▲ **Page 15: [28] Formatted** **Hamal** **3/23/26 6:59:00 PM**

Font: Not Bold

▲ **Page 15: [28] Formatted** **Hamal** **3/23/26 6:59:00 PM**

Font: Not Bold

▲ **Page 15: [28] Formatted** **Hamal** **3/23/26 6:59:00 PM**

Font: Not Bold

▲ **Page 15: [28] Formatted** **Hamal** **3/23/26 6:59:00 PM**

Font: Not Bold

▲ **Page 15: [28] Formatted** **Hamal** **3/23/26 6:59:00 PM**

Font: Not Bold

▲ **Page 15: [28] Formatted** **Hamal** **3/23/26 6:59:00 PM**

Font: Not Bold

▲ **Page 15: [28] Formatted** **Hamal** **3/23/26 6:59:00 PM**

Font: Not Bold

▲ **Page 15: [29] Deleted** **Hamal** **3/24/26 11:17:00 AM**

▼ **Page 15: [29] Deleted** **Hamal** **3/24/26 11:17:00 AM**

▲ **Page 15: [29] Deleted** **Hamal** **3/24/26 11:17:00 AM**

▼ **Page 15: [29] Deleted** **Hamal** **3/24/26 11:17:00 AM**

▲ **Page 15: [29] Deleted** **Hamal** **3/24/26 11:17:00 AM**

▼ **Page 15: [29] Deleted** **Hamal** **3/24/26 11:17:00 AM**

▲ **Page 15: [30] Deleted** **Hamal** **3/23/26 5:29:00 PM**

▼
▲
Page 15: [30] Deleted **Hamal** **3/23/26 5:29:00 PM**

▼
▲
Page 15: [30] Deleted **Hamal** **3/23/26 5:29:00 PM**

▼
▲
Page 15: [30] Deleted **Hamal** **3/23/26 5:29:00 PM**

▼
▲
Page 15: [30] Deleted **Hamal** **3/23/26 5:29:00 PM**

▼
▲
Page 16: [31] Formatted **Hamal** **3/24/26 1:48:00 PM**

Font: Not Bold

▼
▲
Page 16: [31] Formatted **Hamal** **3/24/26 1:48:00 PM**

Font: Not Bold

▼
▲
Page 16: [32] Formatted **Hamal** **3/24/26 1:48:00 PM**

Font: Not Bold

▼
▲
Page 16: [32] Formatted **Hamal** **3/24/26 1:48:00 PM**

Font: Not Bold

▼
▲
Page 16: [32] Formatted **Hamal** **3/24/26 1:48:00 PM**

Font: Not Bold

▼
▲
Page 16: [33] Deleted **Hamal** **3/20/26 1:02:00 PM**

▼
▲
Page 16: [33] Deleted **Hamal** **3/20/26 1:02:00 PM**

▼
▲
Page 16: [33] Deleted **Hamal** **3/20/26 1:02:00 PM**

▼
▲
Page 16: [34] Deleted **Hamal** **3/20/26 1:02:00 PM**

▼
▲
Page 16: [34] Deleted **Hamal** **3/20/26 1:02:00 PM**

▲
Page 16: [34] Deleted **Hamal** **3/20/26 1:02:00 PM**

▼
▲
Page 16: [34] Deleted **Hamal** **3/20/26 1:02:00 PM**

▼
▲
Page 16: [35] Deleted **Hamal** **3/20/26 1:03:00 PM**

▼
▲
Page 16: [35] Deleted **Hamal** **3/20/26 1:03:00 PM**

▼
▲
Page 16: [35] Deleted **Hamal** **3/20/26 1:03:00 PM**

▼
▲
Page 16: [35] Deleted **Hamal** **3/20/26 1:03:00 PM**

▼
▲
Page 16: [36] Deleted **Hamal** **3/9/26 8:58:00 AM**

▼
▲
Page 16: [36] Deleted **Hamal** **3/9/26 8:58:00 AM**

▼
▲
Page 16: [36] Deleted **Hamal** **3/9/26 8:58:00 AM**

▼
▲
Page 16: [37] Deleted **Hamal** **3/20/26 8:26:00 AM**

▼
▲
Page 16: [37] Deleted **Hamal** **3/20/26 8:26:00 AM**

▼
▲
Page 16: [37] Deleted **Hamal** **3/20/26 8:26:00 AM**

▼
▲
Page 16: [37] Deleted **Hamal** **3/20/26 8:26:00 AM**

▼
▲
Page 16: [37] Deleted **Hamal** **3/20/26 8:26:00 AM**

▼
▲
Page 18: [38] Formatted Hamal 3/24/26 1:48:00 PM

Font: Not Bold, Italic

▲
Page 18: [38] Formatted Hamal 3/24/26 1:48:00 PM

Font: Not Bold, Italic

▲
Page 18: [38] Formatted Hamal 3/24/26 1:48:00 PM

Font: Not Bold, Italic

▲
Page 18: [39] Formatted Hamal 3/24/26 1:48:00 PM

Font: Not Bold

▲
Page 18: [39] Formatted Hamal 3/24/26 1:48:00 PM

Font: Not Bold

▲
Page 18: [40] Deleted Hamal 3/20/26 1:01:00 PM

✖
▲

Page 18: [40] Deleted Hamal 3/20/26 1:01:00 PM

✖
▲

Page 18: [40] Deleted Hamal 3/20/26 1:01:00 PM

✖
▲

Page 18: [41] Formatted Hamal 3/24/26 1:48:00 PM

English (UK)

▲
Page 18: [41] Formatted Hamal 3/24/26 1:48:00 PM

English (UK)

▲
Page 18: [41] Formatted Hamal 3/24/26 1:48:00 PM

English (UK)

▲
Page 18: [42] Formatted Hamal 3/24/26 1:48:00 PM

Not Superscript/ Subscript

▲
Page 18: [42] Formatted Hamal 3/24/26 1:48:00 PM

Not Superscript/ Subscript

▲
Page 18: [43] Deleted Hamal 2/16/26 2:26:00 PM

▼
▲

Page 18: [43] Deleted Hamal 2/16/26 2:26:00 PM



Page 20: [44] Deleted Hamal 3/23/26 5:29:00 PM



Page 20: [44] Deleted Hamal 3/23/26 5:29:00 PM



Page 20: [44] Deleted Hamal 3/23/26 5:29:00 PM



Page 20: [44] Deleted Hamal 3/23/26 5:29:00 PM



Page 20: [44] Deleted Hamal 3/23/26 5:29:00 PM



Page 20: [44] Deleted Hamal 3/23/26 5:29:00 PM



Page 20: [44] Deleted Hamal 3/23/26 5:29:00 PM



Page 20: [44] Deleted Hamal 3/23/26 5:29:00 PM



Page 20: [44] Deleted Hamal 3/23/26 5:29:00 PM



Page 20: [44] Deleted Hamal 3/23/26 5:29:00 PM



Page 20: [44] Deleted Hamal 3/23/26 5:29:00 PM



Page 20: [45] Deleted Hamal 3/23/26 5:29:00 PM



Page 20: [45] Deleted Hamal 3/23/26 5:29:00 PM



▲ Page 20: [45] Deleted Hamal 3/23/26 5:29:00 PM

▼

▲ Page 20: [45] Deleted Hamal 3/23/26 5:29:00 PM

▼

▲ Page 20: [45] Deleted Hamal 3/23/26 5:29:00 PM

▼

▲ Page 20: [46] Deleted Hamal 3/23/26 5:29:00 PM

▼

▲ Page 20: [46] Deleted Hamal 3/23/26 5:29:00 PM

▼

▲ Page 20: [46] Deleted Hamal 3/23/26 5:29:00 PM

▼

▲ Page 20: [46] Deleted Hamal 3/23/26 5:29:00 PM

▼

▲ Page 20: [46] Deleted Hamal 3/23/26 5:29:00 PM

▼

▲ Page 22: [47] Deleted Hamal 4/8/26 11:04:00 AM

▼

▲ Page 23: [48] Deleted Hamal 2/16/26 2:26:00 PM

▼

▲ Page 23: [48] Deleted Hamal 2/16/26 2:26:00 PM

▼

▲ Page 23: [49] Deleted Hamal 3/23/26 5:29:00 PM

▼

▲ Page 23: [49] Deleted Hamal 3/23/26 5:29:00 PM

▼

▲ Page 23: [49] Deleted Hamal 3/23/26 5:29:00 PM

▼

▲ Page 23: [49] Deleted Hamal 3/23/26 5:29:00 PM

▼

▼
▲
Page 23: [49] Deleted **Hamal** **3/23/26 5:29:00 PM**

▼
▲
Page 23: [49] Deleted **Hamal** **3/23/26 5:29:00 PM**

▼
▲
Page 23: [49] Deleted **Hamal** **3/23/26 5:29:00 PM**

▼
▲
Page 23: [50] Deleted **Hamal** **3/23/26 5:29:00 PM**

▼
▲
Page 23: [50] Deleted **Hamal** **3/23/26 5:29:00 PM**

▼
▲
Page 23: [50] Deleted **Hamal** **3/23/26 5:29:00 PM**

▼
▲
Page 23: [50] Deleted **Hamal** **3/23/26 5:29:00 PM**

▼
▲
Page 23: [50] Deleted **Hamal** **3/23/26 5:29:00 PM**

▼
▲
Page 23: [51] Deleted **Hamal** **3/23/26 5:29:00 PM**

▼
▲
Page 23: [51] Deleted **Hamal** **3/23/26 5:29:00 PM**

▼
▲
Page 23: [51] Deleted **Hamal** **3/23/26 5:29:00 PM**

▼
▲
Page 23: [51] Deleted **Hamal** **3/23/26 5:29:00 PM**

▼
▲
Page 23: [51] Deleted **Hamal** **3/23/26 5:29:00 PM**

▼
▲
Page 23: [51] Deleted **Hamal** **3/23/26 5:29:00 PM**

Page 24: [52] Formatted **Hamal** **3/18/26 12:24:00 PM**

Justified, Space Before: 0 pt, After: 0 pt, Line spacing: 1.5 lines

▲ **Page 24: [53] Deleted** **Hamal** **3/18/26 12:24:00 PM**

▼

▲ **Page 25: [54] Deleted** **Hamal** **2/10/26 8:44:00 AM**

▼

▲ **Page 27: [55] Formatted** **Hamal** **3/23/26 10:42:00 AM**

English (UK)

▲ **Page 27: [55] Formatted** **Hamal** **3/23/26 10:42:00 AM**

English (UK)

▲ **Page 27: [55] Formatted** **Hamal** **3/23/26 10:42:00 AM**

English (UK)

▲ **Page 27: [56] Formatted** **Hamal** **3/24/26 1:44:00 PM**

Font: Not Bold, Italic

▲ **Page 27: [56] Formatted** **Hamal** **3/24/26 1:44:00 PM**

Font: Not Bold, Italic

▲ **Page 27: [56] Formatted** **Hamal** **3/24/26 1:44:00 PM**

Font: Not Bold, Italic

▲ **Page 27: [57] Formatted** **Hamal** **3/24/26 1:44:00 PM**

Font: Not Bold

▲ **Page 27: [57] Formatted** **Hamal** **3/24/26 1:44:00 PM**

Font: Not Bold

▲ **Page 27: [58] Formatted** **Hamal** **3/24/26 1:44:00 PM**

Font: Not Bold

▲ **Page 27: [58] Formatted** **Hamal** **3/24/26 1:44:00 PM**

Font: Not Bold

▲ **Page 29: [59] Formatted** **Hamal** **3/24/26 11:06:00 AM**

Font: Not Bold

▲ **Page 29: [59] Formatted** **Hamal** **3/24/26 11:06:00 AM**

Font: Not Bold

▲
Page 29: [59] Formatted **Hamal** **3/24/26 11:06:00 AM**

Font: Not Bold

▲
Page 29: [59] Formatted **Hamal** **3/24/26 11:06:00 AM**

Font: Not Bold

▲
Page 29: [59] Formatted **Hamal** **3/24/26 11:06:00 AM**

Font: Not Bold

▲
Page 29: [59] Formatted **Hamal** **3/24/26 11:06:00 AM**

Font: Not Bold

▲
Page 29: [59] Formatted **Hamal** **3/24/26 11:06:00 AM**

Font: Not Bold

▲
Page 29: [59] Formatted **Hamal** **3/24/26 11:06:00 AM**

Font: Not Bold

▲
Page 29: [60] Formatted **Hamal** **3/24/26 11:06:00 AM**

Font: Not Bold, English (UK)

▲
Page 29: [60] Formatted **Hamal** **3/24/26 11:06:00 AM**

Font: Not Bold, English (UK)

▲
Page 29: [61] Formatted **Hamal** **3/24/26 1:45:00 PM**

English (UK)

▲
Page 29: [61] Formatted **Hamal** **3/24/26 1:45:00 PM**

English (UK)

▲
Page 29: [61] Formatted **Hamal** **3/24/26 1:45:00 PM**

English (UK)

▲
Page 29: [62] Formatted **Hamal** **3/24/26 11:06:00 AM**

Font: Not Bold, English (UK)

▲
Page 29: [62] Formatted **Hamal** **3/24/26 11:06:00 AM**

Font: Not Bold, English (UK)

▲
Page 29: [63] Formatted **Hamal** **3/24/26 1:45:00 PM**

English (UK)

▲

Page 29: [63] Formatted **Hamal** **3/24/26 1:45:00 PM**

English (UK)

▲
Page 29: [63] Formatted **Hamal** **3/24/26 1:45:00 PM**

English (UK)

▲
Page 29: [64] Formatted **Hamal** **3/24/26 11:06:00 AM**

Font: Not Bold

▲
Page 29: [64] Formatted **Hamal** **3/24/26 11:06:00 AM**

Font: Not Bold

▲
Page 29: [64] Formatted **Hamal** **3/24/26 11:06:00 AM**

Font: Not Bold

▲
Page 29: [64] Formatted **Hamal** **3/24/26 11:06:00 AM**

Font: Not Bold

▲
Page 29: [64] Formatted **Hamal** **3/24/26 11:06:00 AM**

Font: Not Bold

▲
Page 29: [64] Formatted **Hamal** **3/24/26 11:06:00 AM**

Font: Not Bold

▲
Page 29: [64] Formatted **Hamal** **3/24/26 11:06:00 AM**

Font: Not Bold

▲
Page 29: [64] Formatted **Hamal** **3/24/26 11:06:00 AM**

Font: Not Bold

▲
Page 29: [64] Formatted **Hamal** **3/24/26 11:06:00 AM**

Font: Not Bold

▲
Page 29: [64] Formatted **Hamal** **3/24/26 11:06:00 AM**

Font: Not Bold

▲
Page 29: [64] Formatted **Hamal** **3/24/26 11:06:00 AM**

Font: Not Bold

▲
Page 29: [64] Formatted **Hamal** **3/24/26 11:06:00 AM**

Font: Not Bold

▲
Page 29: [64] Formatted **Hamal** **3/24/26 11:06:00 AM**

Font: Not Bold

▲ **Page 29: [64] Formatted** **Hamal** **3/24/26 11:06:00 AM**

Font: Not Bold

▲ **Page 29: [64] Formatted** **Hamal** **3/24/26 11:06:00 AM**

Font: Not Bold

▲ **Page 29: [64] Formatted** **Hamal** **3/24/26 11:06:00 AM**

Font: Not Bold

▲ **Page 29: [64] Formatted** **Hamal** **3/24/26 11:06:00 AM**

Font: Not Bold

▲ **Page 29: [65] Deleted** **Hamal** **3/24/26 1:46:00 PM**

▼
▲

Page 29: [65] Deleted **Hamal** **3/24/26 1:46:00 PM**

▼
▲

Page 29: [65] Deleted **Hamal** **3/24/26 1:46:00 PM**

▼
▲

Page 29: [66] Formatted **Hamal** **3/24/26 11:06:00 AM**

Font: Not Bold

▲ **Page 29: [66] Formatted** **Hamal** **3/24/26 11:06:00 AM**

Font: Not Bold

▲ **Page 29: [67] Deleted** **Hamal** **3/20/26 4:05:00 PM**

▼
▲

Page 29: [67] Deleted **Hamal** **3/20/26 4:05:00 PM**

▼
▲

Page 29: [67] Deleted **Hamal** **3/20/26 4:05:00 PM**

▼
▲

Page 29: [68] Deleted **Hamal** **3/23/26 5:29:00 PM**

▼
▲

Page 29: [68] Deleted **Hamal** **3/23/26 5:29:00 PM**

▼

▲
Page 29: [68] Deleted **Hamal** **3/23/26 5:29:00 PM**

▼

▲
Page 29: [68] Deleted **Hamal** **3/23/26 5:29:00 PM**

▼

▲
Page 29: [68] Deleted **Hamal** **3/23/26 5:29:00 PM**

▼

▲
Page 29: [68] Deleted **Hamal** **3/23/26 5:29:00 PM**

▼

▲
Page 29: [68] Deleted **Hamal** **3/23/26 5:29:00 PM**

▼

▲
Page 30: [69] Deleted **Hamal** **3/20/26 11:12:00 AM**

▼

▲
Page 30: [69] Deleted **Hamal** **3/20/26 11:12:00 AM**

▼

▲
Page 30: [69] Deleted **Hamal** **3/20/26 11:12:00 AM**

▼

▲
Page 30: [70] Formatted **Hamal** **3/20/26 11:17:00 AM**

Font: Font color: Auto

▲
Page 30: [70] Formatted **Hamal** **3/20/26 11:17:00 AM**

Font: Font color: Auto

▲
Page 30: [70] Formatted **Hamal** **3/20/26 11:17:00 AM**

Font: Font color: Auto

▲
Page 30: [70] Formatted **Hamal** **3/20/26 11:17:00 AM**

Font: Font color: Auto

▲
Page 30: [70] Formatted **Hamal** **3/20/26 11:17:00 AM**

Font: Font color: Auto

▲
Page 30: [71] Deleted **Hamal** **3/20/26 11:19:00 AM**

▲ Page 30: [71] Deleted Hamal 3/20/26 11:19:00 AM

▲ Page 30: [72] Deleted Hamal 3/20/26 4:05:00 PM

▼
▲ Page 30: [72] Deleted Hamal 3/20/26 4:05:00 PM

▼
▲ Page 30: [73] Deleted Hamal 3/24/26 4:03:00 PM

▼
▲ Page 30: [73] Deleted Hamal 3/24/26 4:03:00 PM

▼
▲ Page 30: [74] Deleted Hamal 3/24/26 4:03:00 PM

▼
▲ Page 30: [74] Deleted Hamal 3/24/26 4:03:00 PM

▼
▲ Page 30: [74] Deleted Hamal 3/24/26 4:03:00 PM

▼
▲ Page 30: [75] Deleted Hamal 3/24/26 4:06:00 PM

▼
▲ Page 30: [75] Deleted Hamal 3/24/26 4:06:00 PM

▼
▲ Page 30: [76] Deleted Hamal 3/20/26 11:40:00 AM

▼
▲ Page 30: [76] Deleted Hamal 3/20/26 11:40:00 AM

▼
▲ Page 30: [76] Deleted Hamal 3/20/26 11:40:00 AM

▼
▲ Page 30: [76] Deleted Hamal 3/20/26 11:40:00 AM

▲

▼
▲
Page 30: [77] Deleted **Hamal** **3/24/26 4:08:00 PM**

▼
▲
Page 30: [77] Deleted **Hamal** **3/24/26 4:08:00 PM**

▼
▲
Page 30: [77] Deleted **Hamal** **3/24/26 4:08:00 PM**

▼
▲
Page 30: [78] Deleted **Hamal** **3/20/26 4:05:00 PM**

▼
▲
Page 30: [78] Deleted **Hamal** **3/20/26 4:05:00 PM**

▼
▲
Page 30: [78] Deleted **Hamal** **3/20/26 4:05:00 PM**